STUDY OF EVAPORATED AMORPHOUS SILICON FILMS BY FREQUENCY DEPENDENT CONDUCTIVITY AND PHASE SHIFT ANALYSIS OF MODULATED PHOTOCURRENT METHODS

by

Celal Zaim ÇİL

B.S. in E.E., Boğaziçi University, 1982

M.S. in E.E., Boğaziçi University, 1984

Submitted to the Institute for Graduate Studies in Science and Engineering in partial fulfillment of the requirements for the degree of

Doctor

of

Philosophy

Bogazici University Library

39001100310468 14

Boğaziçi University

1989

ACKNOWLEDGEMENTS

I have been extremely fortunate in having the help of many people during the course of this thesis.

I would especially like to thank Assoc.Prof.Dr.Gülen Aktaş without whom this work could not have been possible. Her patience,encouragement, and constant help were invaluable.

I would like to thank Prof.Dr.Sabih Tansal for his guidance and encouragement.

In particular, I would like to thank Dr.Ender Aktulga for his extremely useful help.

I also want to thank Assoc.Prof.Dr.Yani Skarlatos for his suggestions, guidance and critical reading of the manuscript.

I want to express my sincere thanks to Dr.İsa Eşme for his suggestions and assistance in drawing some of the figures.

I would like to express my appreciation to my wife, Ayşen, and my children İpek and Emir Şahin for their patiance during this work.

My final thanks are due to all members of Physics Department who offer a very friendly environment during the four years. My special thanks go to Professors Ömür Akyüz, Haluk Beker, Meral Serdaroğlu, Cihan Saçlıoğlu, and Metin Arık.

STUDY OF EVAPORATED AMORPHOUS SILICON FILMS BY FREQUENCY DEPENDENT CONDUCTIVITY AND PHASE SHIFT ANALYSIS OF MODULATED PHOTOCURRENT METHODS

A.c. and d.c. conductivity measurements have been performed on amorphous silicon films produced by electron gun evaporation. The a.c. measurements have been performed at frequencies between 100 Hz and 2 MHz, and at temperatures between 150K and 400K. The d.c. behavior of the samples obey the $T^{-1/4}$ law between 77K and 250K. The a.c. conductivity of the films are well represented by the form Aw^{s}, where A and s are determined to be temperature dependent parameters. The data are discussed in terms of classical models based on pair approximation and a unified theory, the extended pair approximation, EPA. Although the a.c. behavior can be approximately explained by the Correlated Barrier Hopping model below 200K, the temperature and the frequency dependence are stronger than any classical model predicts. The a.c. data show a perfect agreement with the quasi-universal law predicted by the EPA calculations. However, quantitative calculations with the EPA results give unreasonable values for both the decay parameter α, and the rate parameter R_o.

One of the major problems of the method of Phase shift analysis of modulated photocurrent, PSAMP, for studying the

density of states in the energy gap of amorphous semiconductors has been the determination of the energy scale corresponding to this DOS profile. A new way of dealing with this problem is presented. A computer analysis is used to confirm the validity of this method and to demonstrate how it can be used.

A simulation that is used to determine the sensitivity of the PSAMP method to the differences in the fine scale structures in the DOS distributions is presented. Four DOS distributions are considered and the expected data are obtained. The results show that the PSAMP method is very sensitive to such fine features in the DOS distributions. A comparison is also made with the sensitivity of other techniques commonly used in the determination of the DOS profiles.

BUHARLAŞMA YÖNTEMİYLE ELDE EDİLEN AMORF SİLİSYUM FİLMLERİN FREKANS BAĞIMLI İLETKENLİK VE MODÜLE EDİLMİŞ FOTOAKIMIN FAZ FARKI ANALİZİ YÖNTEMLERİYLE İNCELENMESİ

Bu çalışmanın ilk bölümünde, elektron tabancası yöntemiyle buharlaştırılmış amorf silisyum filmlerin a.a. ve d.a. iletkenlik ölçümleri yapılmıştır. A.a. ölçümleri 100 Hz ve 2 MHz frekans aralığında ve 150K ile 400K sıcaklık aralığında gerçekleştirilmiştir. Örneklerin d.a. davranışı 77K ve 250K arasında $T^{-1/4}$ yasasına uymaktadır. A.a. iletkenliği Aw^{s} şeklinde bir bağıntıya iyi bir şekilde uymaktadır. Burada A ve s'nin sıcaklığa bağımlı parametreler oldukları belirlenmiştir. Ölçme sonuçları çift yaklaşımına dayanan klasik modeller ve birleştirilmiş bir kuram olan genişletilmiş çift yaklaşımı modeline (EPA) göre incelenmiştir. 200K sıcaklığın altında a.a. davranışı İlişkili Engel Hoplaması modeli ile yaklaşık olarak izah edilebilse bile frekans ve sıcaklık bağımlılığı hiç bir klasik modelin öngörmediği kadar yüksektir. A.a. ölçme sonuçları EPA hesaplarının öngördüğü evrensel yasayla çok iyi bir uyum göstermiştir. Ancak, EPA sonuçlarına dayalı detaylı sayısal hesaplar hem sönüm parametresi α, hem de sıklık parametresi R_o için makul olmayan sonuçlar vermiştir.

Modüle edilmiş fotoakımın faz kayması analizi, PSAMP, metodunun en önemli problemlerinden birisi de band aralığındaki

durum yoğunluğu, DOS, incelemelerinde bu durum yoğunluğu dağılımına karşı gelen enerji ekseninin belirlenmesidir. Bu problemin çözümü için yeni bir yol önerilmiştir. Bu metodun geçerliliğini doğrulamak ve yöntemin nasıl kullanılacağını göstermek için bir bilgisayar analizi kullanılmıştır.

PSAMP metodunun durum yoğunluğu dağılımındaki küçük ölçüdeki değişimlere karşı hassasiyetini ve ayırım gücünü belirlemek için bir simülasyon kullanılmıştır. Dört ayrı durum yoğunluğu dağılımı gözönüne alınmış ve bunlardan beklenen veriler elde edilmiştir. Sonuçlar PSAMP metodunun durum yoğunluğu dağılımındaki çok küçük değişimlere karşı çok hassas olduğunu göstermiştir. Durum yoğunluğu dağılımı belirlemede çokca kullanılan diğer yöntemlerin hassasiyetiyle de bir karşılaştırma yapılmıştır.

TABLE OF CONTENTS

	Page
ACKNOWLEDGEMENTS	iii
ABSTRACT	v
ÖZET	vii
LIST OF FIGURES	x
LIST OF TABLES	xiii
I. INTRODUCTION	1
II. THEORY	5
A. Structure of Tetrahedrally-Bonded Amorphous Semiconductors	5
B. Characterization of Amorphous Semiconductors	10
1. Temperature Dependence of D.C. Conductivity	10
2. A.C. Conductivity	12
a. Models for Frequency Dependent Conductivity -The Pair Approximation	12
(1). Quantum Mechanical Tunneling (QMT) Model	16
(2). Correlated Barrier Hopping (CBH) Model	18
b. Unified Models-Extended Pair Approximation--EPA	21
III. EXPERIMENTAL TECHNIQUES	25
A. Preparation of the Films	25
B. Experimental Setup	28
C. D.C. Measurements	29
D. A.C. Measurements	30
IV. EXPERIMENTAL RESULTS AND DISCUSSION	33
V. CHARACTERIZATION OF AMORPHOUS SEMICONDUCTORS BY PHOTOCONDUCTIVITY MEASUREMENTS	48
A. Phase Shift Analysis of Modulated Photocurrent (PSAMP) Method	48
B. A New Approach to Determining the Energy Scale	53
C. Sensitivity Analysis of the PSAMP Method	66
VI. CONCLUSION	79
BIBLIOGRAPHY	82

LIST OF FIGURES

		Page
FIGURE (1)	Various forms proposed for the density of states in amorphous semiconductors. Localized states are shown shaded. (a) Overlapping conduction and valence band tails as proposed by Cohen et al.(16), the CFO model. (b) A real gap in the density of states, suggested as being appropriate for a CRN without defects.	9
FIGURE (2)	Illustration of the temperature dependence of conductivity expected on the model of Figure (1).	11
FIGURE (3)	Schematic representation of pair of two defect states (1-D). (a) in equilibrium (b) after the application of the electric field, ε . Here W is the maximum barrier height, Δ is the energy separation between states 1 and 2, $e\varepsilon R$ is the energy shift due to applied field .	14
FIGURE (4)	Model for overlapping Coulomblike potential wells for charged centers. The ground state energy is Wm, the potential separating these states is W, the potentials are centered a distance R apart, and the energy difference between two sites is denoted by Δ .	23
FIGURE (5)	Scaled EPA conductivities for five models.	23
FIGURE (6)	Masks used for obtaining amorphous silicon samples in coplanar geometry: a) silicon mask, b) electrode mask, c) cross-section of the prepared sample.	26
FIGURE (7)	Block diagram of the d.c. measurement system.	30
FIGURE (8)	Temperature dependence of pure a.c. conductivity at the indicated frequencies, and d.c. conductivity of one of the samples. The dashed lines are drawn as a guide to eye for a linear relationship below 200K.	34
FIGURE (9)	Frequency dependence of pure a.c. conductivity of one of the samples at indicated temperatures.	35

Page

FIGURE (10) s-values plotted against temperature scaled to the large polaron activation energy. The line is calculated from the polaron tunneling model for W_o = 0.6 eV, and $2\alpha r_o$ = 0.6, $\tau_p = 10^{-12}$s, and f = 32 kHz. 40

FIGURE (11) Inverse temperature dependence of d.c. conductivities for four samples. 42

FIGURE (12) D.c. conductivities of four samples as plotted against $T^{-1/4}$. 43

FIGURE (13) Reduced frequency-dependent conductivity against reduced frequency for sample-2. 44

FIGURE (14) Reduced frequency-dependent conductivity against reduced frequency for sample-5. 45

FIGURE (15) Energy level scheme for the analysis of the PSAMP method. 49

FIGURE (16) The density of state distribution used in the simulation. 57

FIGURE (17) Modulation frequency dependence of the phase shift values for several temperatures. 58

FIGURE (18) Modulation frequency dependence of the intensity of photocurrent values for several temperatures. 58

FIGURE (19) Determination of $Nc\sigma\nu$ graphically. The solid line represents Equation (5.21) with ω_p = 70 Hz, T_1 = 300K, and T_2 = 320K. γ spectra at these two temperatures are superimposed on this line. Dashed lines represent (a) γ_{1p} corresponding to 70 Hz, (b) the equivalent ω_q, (c) the equivalent γ_{2q}, and (d) the corresponding value of $Nc\sigma\nu$. 59

FIGURE (20) Determination of $Nc\sigma\nu$ graphically from γ spectra at temperatures 300K and 340K. 60

FIGURE (21) Modulation frequency dependence for α's at different temperatures. The dashed lines show the determination of the normalization coefficient (α_1/α_2) for C_2 which corresponds to T_2 = 320K for arbitrarily chosen C_1 value at T_1 = 300K. 62

FIGURE (22) Final energetic distribution of density of states obtained by using the procedure described in the text. The NcC values used at each temperature are indicated. 63

Page

FIGURE (23) Energetic distribution of density of states for the case where N_cC is taken to be ($1x10^{30}$) for all M(Enj) calculations. 64

FIGURE (24) The distribution of density of states for an a-Si:N alloy film. The curve on the left is the original curve of White et al.(45), and the curve on the right represents the DOS distribution obtained by the method described in the text. 65

FIGURE (25) Four density of states distributions used in the simulation(49). 67

FIGURE (26) Modulation frequency dependence of the calculated phase shift values for 250K. 69

FIGURE (27) Modulation frequency dependence of the calculated phase shift values for 330K. 70

FIGURE (28) Modulation frequency dependence of the calculated photocurrent values for 250K. 71

FIGURE (29) Modulation frequency dependence of the calculated photocurrent values for 330K. 72

FIGURE (30) Final energetic distributions of M(E) for four DOS distributions. The same energy for the original DOS distributions are shown in the inset. 75

FIGURE (31) Field effect "data" generated from the DOS curves of Figure (25),(49). 76

FIGURE (32) DOS distributions used in the simulation for the C-V method(49). 77

FIGURE (33) C-V "data" generated from the DOS curves of Figure (32),(49). 78

LIST OF TABLES

Page

TABLE 1. Experimentally determined a.c. conductivities and s values and those calculated according to Equations (2.34) and (4.4) at 32 kHz. For each sample $\sigma(\omega,T)$ value measured at the lowest temperature is used to scale the other calculated $\sigma(\omega,T)$ values. The parameters used in the calculations are W_m=1,2 eV, $\tau_o=10^{-12}$ sec, Δ_o=0.1 eV, and κ=3. 38

TABLE 2. The EPA d.c. results. α^{-1} is taken to be 10 Å in the calculations. 47

I. INTRODUCTION

In recent years a remarkable progress has been made in both physics and technologies of amorphous semiconductors. Twenty years ago, amorphous semiconducting devices were a radical concept. Although their technologies are still at a fairly early stage of development, recent commercial devices and others on the way assure the future of amorphous semiconductors.

A major advantage of amorphous over crystalline technology is dramatically reduced cost, without which, some applications such as the inexpensive solar cells that provide power for pocket calculators would not be economically feasible. But other applications are now far more significant: high-powered solar cells, the thin film transistor arrays that drive the latest generation of liquid-crystal color television and graphics displays, electrophotographic drums, gas sensors, and image arrays(1).

The term amorphous is used for materials prepared in the form of a thin film on a relatively cold substrate to prevent crystallization.

Of all amorphous materials hydrogenated-amorphous silicon, a-Si:H, has some unique physical properties and remarkable advantages, some of which can be summarized as:

(a) high optical absorption and large photoconductivity in the visible region;

(b) an existence of valency electron controllability, that is, dopability;

(c) low cost;

(d) large area non-epitaxial growth on any substrate material at low temperature.

One of the most important problems in the study on amorphous semiconductors is strong dependence of observed electrical and optical properties on the preparation methods and conditions of the films. The large characteristic spectrum observed on the films prepared by evaporation, sputtering or glow-discharge methods have generally been tried to be interpreted according to the Density of States (DOS) distributions in the band gap. Hence, determining the distribution of the density of localized states in the band gap with respect to energy becomes very important in investigating the amorphous semiconductors. But, since the exact structure of these materials is not known and particularly it depends on sample preparation, this distribution has to be determined experimentally.

In the last several years significant advances have been achieved by relating most measured properties of amorphous semiconductors to specific properties of these localized states. Included are most types of transport measurements, photoluminescence, spin properties, and optical absorption.

Among transport measurements, d.c. and a.c. conductivity are the two relatively straightforward measurements, which give information about the density of states around the Fermi energy, $N(E_F)$.

The most widely used techniques in determining the DOS distribution in the band gap have been the transient methods like TSCAP(2), ICTS(3), and capacitance DLTS(3), and the steady-state methods like the field-effect(4) and the capacitance-voltage, C-V(5), measurements. All these methods investigate the properties of the space-charge region that forms at the metal-semiconductor interface.

An alternative method to determine a gap state profile is the phase shift analysis of the modulated photocurrent, PSAMP, method(6). In this method localized states are energetically distinguished by their difference in thermal emission rate into the conduction band. The phase shift that exists between a sinusoidally modulated excitation light and the induced photocurrent is closely related to the density of localized states at a particular energy level, which, in turn, is directly associated with the modulation frequency. The magnitude of the modulated photocurrent also depends on the nature of the localized states.

Unlike other methods with a limited application range, like the field-effect and the C-V techniques which can only be applied to a-Si:H or the capacitance DLTS technique which can only be applied to doped amorphous semiconductors(7), the PSAMP method has quite a wide application range and it has been successfully applied to pure(8) and hydrogenated amorphous semiconductors(9) and also to doped crystalline samples(10).

This thesis consists of essentially two parts. In the first part (Chapters II, III, and IV) a.c. and d.c. measurements performed on evaporated amorphous silicon films are presented. An understanting of the transport mechanisms in these samples is tried to be developed through a comparison of the data with some of the a.c. and the d.c. theories.

In Chapter II theories of d.c. and a.c. conductivities are given briefly.

In Chapter III preparation details of the samples, experimental setups, and the measurement techniques are explained.

In Chapter IV the data are presented and discussed in terms of classical models based on the pair approximation and a unified theory, the extended pair approximation, EPA.

The second part of the thesis (Chapter V) is devoted to the PSAMP method. One of the major problems of this method for studying the DOS distribution in the energy gap of amorphous semiconductors has been the determination of the energy scale corresponding to this DOS profile. A new way of dealing with this problem is presented(11). This new method is especially useful in the case where the DOS profile lacks a characteristic peak. A computer analysis is used to confirm the validity of this method and to demonstrate how it can be used.

In the second simulation a sensitivity analysis of the PSAMP method to the differences in the fine scale structures in the DOS distributions is made(12). Then a comparison is made with the sensitivity of other methods to these fine scale features in the DOS profile.

II. THEORY

A. Structure of Tetrahedrally-Bonded Amorphous Semiconductors

In a perfect crystalline material the order of atoms is determined by atomic configuration in the unit cell and by three linearly-independent translational vectors. In a real crystalline material, there are many defects such as impurities, dislocations and voids. For many cases, these defects can be considered as scattering centers for electrons, and the transport mechanisms can be explained by Boltzmann Theory. In crystalline materials, assuming a perfect crystal and neglecting the effect of phonons, each electron is described by a Bloch wavefunction. Band structure and effective mass for electrons or holes are then determined for a perfect crystal. Hence, a simple transport mechanism is solved for an ideal crystal and electron dynamics is then considered as a perturbation, that is, deviation from a perfect structure. This is not possible in amorphous materials. First of all the atomic structure of the material is not known. Even for a definite sample, the experiments do not give enough information to determine the atomic structure exactly. Furthermore, even if the locations of all the atoms are known, the calculation of their eigenvalues is impossible. On the

other hand, the randomness is so high that it can not be considered as a perturbation. However, some concepts used in connection with crystals remain useful, even in disordered states.

Electron and x-ray diffraction experiments show that the nearest neighbours to a given atom in amorphous germanium or silicon have spacings and angles that are very similar to those in their crystalline counterparts, though beyond the second nearest neighbour any substantial resemblance to the crystalline situation ceases. Because the energy levels that can be occupied by the other electrons of an atom in a crystal are approximately those of the isolated atom modified by the effects of the nearest neighbouring atoms, it becomes understandable that the energy bands of amorphous and crystalline semiconductors could be similar.

However, the atomic disorder inherent in amorphous semiconductors causes distinct differences between them and crystalline materials. For example, it scatters the charge carriers so that they now have a finite mean free path, instead of the theoretically unlimited free path they have in perfect crystals. When the disorder increases to the extent that the mean free path is approximatelly equal to the interatomic distance, the probability of finding a carrier very far from its home atom decays exponentially with distance, hence, the carriers are then localized. The concept of localization plays an important part in amorphous materials.

The mean free path varies with the charge carrier's energy. The energy at which the mean free path approximately equals the interatomic distance is called the critical energy, and it represents the boundary between localized and non-localized states.

An amorphous semiconductor has many energy states available within the bandgap. But charge carriers within the

band gap move by hopping between the localized states with a very low mobility between 10^{-6} and 10^{-3} cm^2/Vs. Within the conduction and valence bands, transport occurs via extended states with a much higher mobility, of 1 to 10 cm^2/Vs. So, not the absence of states but their very low mobility within the gap gives rise to the band gap in an amorphous semiconductor. Therefore, the gap is more accurately referred to as a mobility gap and its edges as the mobility edges.

The localized states are of two kinds. The first are the tail states, which emanate from the conduction and valence bands because of the amorphous material's disorder. Nothing can be done about them in a given material. The other localized states in the midgap region are caused by broken bonds, mostly by dangling bonds in amorphous silicon, which are the result of processing procedures.

Chemically, the atoms of group IV amorphous semiconductor like silicon and germanium form a tetrahedral structure by saturating their sp^3 orbitals with four nearest neighbours. If we continue this structure we end up with a form which has five-fold, six-fold, seven-fold coordinated atoms, because bond angles are not constant as in crystalline semiconductor. This structure is called a Continuous Random Network (CRN). As the CRN expands, stress is built up in the bonds and this stress increases with further growth of the network. Increasing stresses finally break the network resulting in voids and dangling bonds. In these regions stress and density are reduced and the structure continues to grow evenly until the stress again builds up to a degree that causes the bonds to break. Therefore it is impossible to build a CRN on a macroscopic scale, and an amorphous sample would never have a homogenous atomic network. These materials can only be produced as thin films, since a bulk sample would eventually break down due to the stresses in the bonds.

The numbers of broken bonds and voids are largely dependent on film preparation technique and conditions. There are three basic preparation techniques for amorphous semiconductor films: vacuum evaporation, sputtering(13), glow-discharge decomposition of silane (SiH_4)(14). The specimens prepared by the third method have fewer voids and dangling bonds compared to those prepared by other techniques(15). In this technique the hydrogen in the silane is thought to saturate the dangling bonds in the film. The films are structurally heterogenous when they are deposited on a cold substrate by evaporation or sputtering technique. They contain a network of internal voids and dangling bonds. Therefore, preparation conditions, such as residual ambient pressure, rate of deposition, substrate temperature, evaporant crucible, and purity of evaporant become very important, and to obtain reproducible thin films is difficult.

The density of electron states, N(E), remains a valid concept for non-crystalline as for crystalline materials and its form should be determined experimentally, since theoretically it is impossible to calculate exact N(E) for a definite amorphous semiconductor sample. The question of states in the gap, whether of intrinsic or extrinsic nature, is of considerable importance. Cohen, Fritzsche, and Ovshinsky(16) supposed that the non-crystalline structure would lead to overlapping band tails of localized states as in Figure (1). Those derived from the conduction band would be neutral when empty and those from the valence band neutral when full. In the overlap region they would be charged, leading to centres with unpaired spins. Such overlapping states would pin the Fermi energy. The other principal feature of this model is the existence of mobility edges at energies in the band tails. These are identified with the critical energies separating localized from extended states.

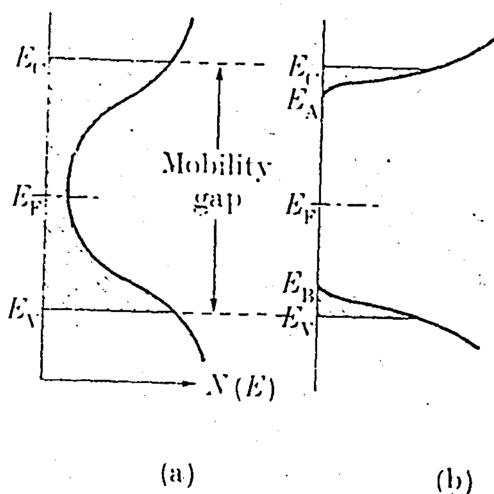

FIGURE (1) Various forms proposed for the density of states in amorphous semiconductors. Localized states are shown shaded. (a) Overlapping conduction and valence band tails as proposed by Cohen et al.(16), the CFO model. (b) A real gap in the density of states, suggested as being appropriate for a CRN without defects.

In evaporated films of Ge and Si and some of their alloys, the conductivity, particularly at low temperatures, is due to hopping conduction between the defect states by electrons with energies near the Fermi level. The density of such states, as we have seen, depends on the conditions of depositions. The characteristic property of amorphous semiconductors is that the Fermi level is located near mid-gap and appears to be pinned. This is not a universal property; indeed Lé Comber and Spear(17), by glow-discharge decomposition of SiH_4 with PH_3 or BH_3 have prepared specimens that are heavily doped, the Fermi energies being shifted towards and

even near to the conduction or valence band. In glasses and perhaps evaporated or sputtered films of Si and Ge, impurities do not normally have this effect, apparently because of the strong tendency to saturate bonds(18). In other words, in these materials each atom can satisfy its valence bonds by adjusting its nearest neighbour environment(19).

B. Characterization of Amorphous Semiconductors

1- Temperature Dependence of D.C. Conductivity

Considering the finite density of states at the mobility edges and around the Fermi level, there are three mechanisms of conduction which we may expect in an amorphous semiconductor in appropriate ranges of temperature(18):

i) transport by carriers excited beyond the mobility edges into non-localized (extended) states at E_c or E_v,

ii) transport by carriers excited into localized states at the mobility edges and hopping at energy level, E_1, in the localized state region near the bands. In this case an activation energy, ω_1, is needed for a carrier to hop.

iii) Since, the DOS at E_F is finite, then there will be a contribution from carriers with energies near E_F which can hop between localized states with an activation energy, ω_2. This process is called as nearest-neighbour hopping.

As the temperature drops more such that kT becomes less than the bandwidth around E_F, another conduction mechanism, which is a characteristic of amorphous semi-conductors, takes place. This mechanism is called as variable-range hopping, in which the d.c. conductivity is given as

$$\sigma(0) = \sigma_0 \exp\left[-\left\{\left(\frac{T_o}{T}\right)^{1/4}\right\}\right] \qquad (2.1)$$

where

$$\sigma_0 = \sqrt{2\pi}\left\{\frac{3}{2}\, e^2 \nu_0\right\}\sqrt{\frac{N(E_f)}{\alpha k T}} \tag{2.2}$$

and

$$T_0 = \frac{16\,\alpha^3}{k\,N(E_f)} \tag{2.3}$$

Here ν_o is the phonon frequency, α^{-1} is the decay length of the localized wavefunction, and k is the Boltzmann constant. In principle, with a reasonable assumption for α, the $N(E_F)$ can be calculated from the slope of the straight line in the $\ln(\sigma(o))$ versus $T^{-1/4}$ plot.

Figure (2) illustrates the temperature dependence of d.c. conductivity expected on the model of Figure (1).

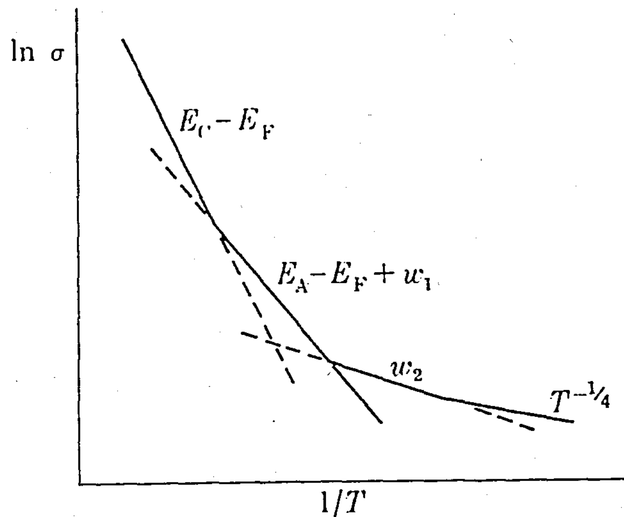

FIGURE (2) Illustration of the temperature dependence of conductivity expected on the model of Figure (1).

2- A.C. Conductivity

A dependence of the real part of the complex conductivity, σ, on frequency in the form of $\sigma = B + A\,\omega^{s}$ where ω is the angular frequency and B is the d.c. limit, has been observed in various kinds of amorphous semiconductors and chalcogenides(20). The earliest theoretical attempt to explain the data was to apply the pair-approximation(21) to the rate equation theory of Miller and Abrahams(22). After obtaining the pure a.c. response, the d.c. conductivity was then added to this to obtain the total frequency dependent response. The variation of A and s with temperature could be partially accounted for by considering different hopping mechanisms in the pair-approximation.

a. Models for Frequency-Dependent Conductivity-The Pair Approximation

Alternating current conductivity measurements are an important means by which deep defect centers may be studied. They are sensitive to processes in which such centers, or groups of centers, develop electron dipole moments under the action of the applied field. The simplest such process to consider involves a pair of centres in close proximity, and the interactions of the applied field with such a pair can in general be relaxation processes. In relaxation events, the exciting field changes the relative environment of a pair of centres, and causes transitions between them governed by the intrinsic relaxation time of the pair, τ. The resultant conductivity is dominated by pairs having relaxation times around ω^{-1}. The random distribution of environments ensures that a wide range of relaxation times will in general be found, and hence the study of a.c. conductivity can give important information about the number and distribution of centres, provided that the mechanism of relaxation is well understood.

Although we will deal with the processes involving electronic relaxation, a similar analysis can be applied to the transfer of atoms between pairs of centers.

In order to help in distinguishing between the various mechanisms, we reserve the term "hopping" for thermal activation of a charge carrier of a pair over the potential barrier between states, and call the process involving the direct coupling due to the overlap of the exponentially decaying wavefunctions of the two sites "tunneling"(20).

The approach which is frequently adopted in calculations of a.c. conductivity is to consider the polarizability of an isolated pair of states and to sum up to contributions due to such pairs to obtain the overall response of the bulk sample. This is generally known as the pair approximation.

All the a.c. models start from the calculation for a pair of single electron states 1 and 2 separated in energy by an amount Δ, and in space by a distance R (Figure (3)) and we assume that the states are occupied by only one electron. If we write the occupation probabilities for the states 1 and 2 as f_1 and f_2 ($f_1+f_2=1$), then the rate equation for electron transfer between the states is

$$\dot{f}_1 = \omega_{21} f_2 - \omega_{12} f_1 = -\dot{f}_2 \tag{2.4}$$

where ω_{21} is the transition rate from the state 2 to the state 1, and ω_{12} is vice versa, and $\dot{f} = df/dt$.

$$\dot{f}_1 = -(\omega_{12} + \omega_{21})\ f_1 + \omega_{21} \tag{2.5}$$

Then, the total average moment of the dipole is

$$P = \frac{e}{V} \quad [x_1 f_1 + x_2 f_2] \tag{2.6}$$

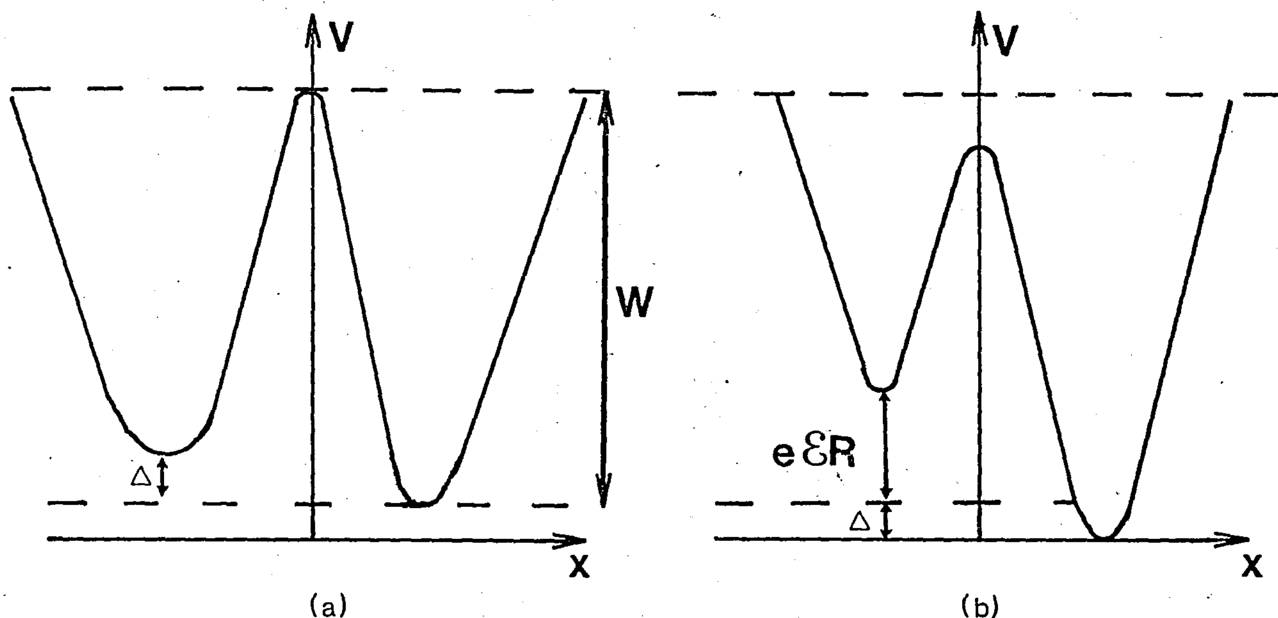

FIGURE (3) Schematic representation of pair of two defect states (1-D). (a) in equilibrium (b) after the application of the electric field, ε . Here W is the maximum barrier height, Δ is the energy separation between states 1 and 2, eεR is the energy shift due to applied field .

where e is the electronic charge, and V is the volume of the sample which is assumed to be unity for convenience. This equation can be put into the form

$$P = e[x_1 f_1 + x_2 - x_2 f_1] \qquad (2.7)$$

and

$$P = eR\cos(\theta) f_1 + ex_2 \qquad (2.8)$$

since $x_1 - x_2 = R \cdot \cos\theta$, where θ is the angle between the direction of the electric field and the axis of the dipole. The current density is given as, $J = dP/dt$.

$$J = eR\cos(\theta)\,\dot{f}_1 \tag{2.9}$$

The occupation probability of the state before the application of an electric field is given by the Fermi-Dirac statistics,

$$f_1(t=o) = \frac{\exp(-W/kT)}{1+\exp(-W/kT)} \tag{2.10}$$

and after the field reaches a steady value, ε, the occupation probability becomes

$$f_1(t\to\infty) \simeq \frac{a\exp(-W/kT)}{1+a\exp(-W/kT)} \tag{2.11}$$

where

$$a \cong 1 - \frac{e\varepsilon R\cos\theta}{kT}$$

Using Equation (2.5),

$$f_1(t) = f_1(o) + [f_1(\infty) - f(o)][1-\exp(-\kappa t)] \tag{2.12}$$

where $\kappa = \omega_{12} + \omega_{12} = \tau^{-1}$.

$$\dot{f}_1(t) = [f_1(\infty) - f_1(o)]\,\kappa\exp(-\kappa t) \tag{2.13}$$

If Equation (2.10), and (2.11) are inserted into (2.13),

$$\dot{f}_1(t) \cong \frac{eR\cos\theta}{kT}\,\frac{\varepsilon}{4\cosh^2(W/2kT)}\cdot\kappa\cdot\exp(-\kappa t) \tag{2.14}$$

Using (2.14) in the (2.9), and applying a harmonic field, $\varepsilon(\omega) = \varepsilon\exp(i\omega t)$, the $y(\omega)$ is given as

$$y(\omega) = \frac{J(\omega)}{\varepsilon(\omega)} = \frac{1}{4}\cdot\frac{e^2R^2\cos^2(\theta)}{kT}\,\frac{1}{\cosh^2(W/2kT)}\left[\frac{\tau^{-1}}{1+i\omega\tau}\right] \tag{2.15}$$

since $Y(\omega) = \sigma_1(\omega) + i\sigma_2(\omega)$, then the real part of it, i.e. the conductivity is

$$\sigma_1(\omega) = \frac{1}{4} \quad \frac{e^2R^2\cos^2\theta}{kT} \quad \frac{\tau^{-1}}{\cosh^2(W/2kT)} \quad \left[\frac{1}{1+\omega^2\tau^2}\right] \cdot \quad (2.16)$$

This $\sigma_1(w)$ is for one dipole and in one direction. For n identical sites, and for $\Delta=0$, the number of dipoles is calculated

$$n = \int N(E) \frac{1}{1+\exp (W/kT)} dW \quad (2.17)$$

$$n \cong N(E_F)\ kT\ \ln 2$$

for a constant N(E) over an energy range kT around E_F. The term $\cos^2\theta$ should be calculated for all directions and by taking the precaution for double counting. The total conductivity is calculated as

$$\sigma_T(\omega) = \frac{N(E_F)\ \ln 2\ e^2R^2}{12} \cdot \frac{\tau^{-1}}{\cosh^2(W/2kT)} \left[\frac{1}{1+\omega^2\tau^2}\right] . \quad (2.18)$$

(1) Quantum Mechanical Tunneling (Q.M.T.) Model

This model has been introduced by Pollak and Geballe (21) and applied to amorphous semiconductors by Austin and Mott(23). If the relaxation process involves an electron surmounting an energy barrier W at a spatial distance R, then the rate with which an electron surmounts the barrier is

$$\frac{1}{\tau} = \nu_{ph} \exp(-W/kT) \exp(-2\alpha R) \quad (2.19)$$

where ν_{ph} is the phonon frequency, W is the barrier height. If an electron tunnels from one state to the other, then the probability of hopping per volume per energy is

$$\frac{P}{V} \doteq \frac{\text{number of hops}}{\text{density of states x energy x volume}} = 1$$

$$1 = \frac{1}{N(E_F)\ kT\ 4\pi R^2 dR} \quad . \tag{2.20}$$

For energies $W \cong kT$, the conductivity for all the relaxation times

$$\sigma_T\ (\omega) = \frac{\pi(N(E_F))^2\ \ kT\ \ln 2\ e^2}{3} \int \left[\frac{\omega}{1+\omega^2\tau^2}\right] R^4 dR \tag{2.21}$$

The term $(\omega/1+\omega^2\tau^2)$ is sharply peaked at $\omega\tau \sim 1$. Therefore the important hops are of the order of $\omega\tau \sim 1$. So, for this ω

$$R_\omega = \frac{1}{2\alpha} \ln \frac{\nu ph}{\omega} \tag{2.23}$$

$$dR = \frac{1}{2\alpha} \frac{d\tau}{\tau} \tag{2.24}$$

are obtained. Since $\tau \cong \frac{1}{\omega}$, then $d\tau \sim 2\tau$, hence

$$dR \cong \frac{1}{\alpha} \tag{2.25}$$

Using this value in the integral with $\omega\tau \cong 1$, the a.c. conductivity is expressed as

$$\sigma(\omega) = \frac{\pi}{96} (eN(E_F))^2\ kT \ln 2\ \ \alpha^{-5}\ \omega \left[\ln \frac{\nu ph}{\omega}\right]^4 \tag{2.26}$$

Equation (2.26) is also known as Austin and Mott formula, and this model is widely called as the Quantum Mechanical Tunneling (QMT) model. In the calculation of this formula multiple hopping is neglected, and also there is no correlation between the hop energy and the hop distance.

The a.c. conductivity can be expressed empirically for the QMT as

$$\sigma(\omega) \propto \omega^{s} T^{n} \tag{2.27}$$

The first important characteristic of conductivity by tunnelling is that the tunneling distance which is given by (2.23) is a function of frequency alone and independent of temperature. Secondly, the ω dependence arises from the $\omega(\ln\frac{\nu_{ph}}{\omega})^4$ term and it is straightforward to show that

$$s = 1 + \frac{4}{\ln(\omega/\nu_{ph})} . \tag{2.28}$$

Note that for this model s is independent of temperature, T. If we assume, following Mott, that ν_{ph} is of the order of an optical phonon frequency ($\sim 10^{13}$ Hz), then for a typical audio-frequency (10^4 Hz) we obtain the value $s \sim 0.8$, which was first observed for impurity states in crystalline semiconductors by Pollak and Geballe(21).

Finally, in the simple single-electron tunneling theory, n=1; that is, the temperature dependence of $\sigma(\omega)$ is linear.

(2) Correlated Barrier Hopping (CBH) Model

In this model for a.c. conductivity, first introduced by Pike (24) and applied by Elliot(25) to a.c. conductivity measurements in chalcogenide films, the charge carrier is assumed to hop between site pairs over the potential barrier separating them. If we consider a single electron hopping between positive defect centers, then the potential barrier will be reduced by the Coulomb interaction, Figure (4), and it is easy to show that the barrier height W is correlated with the separation R according to

$$W = W_m - \frac{e^2}{\pi \kappa R} \tag{2.29}$$

Where $\kappa = \epsilon\epsilon_0$, being the background dielectric constant of the material, and W_m is the energy required to remove the electron from the site into extended states completely.

For electron pairs hopping between defect centres, however, as in the calculations of(25), the barrier lowering for a pair is of the order of

$$W = W_m - \frac{2e^2}{\pi\kappa R} \tag{2.30}$$

and hence, the calculations are similar to those applicable in the single electron case.

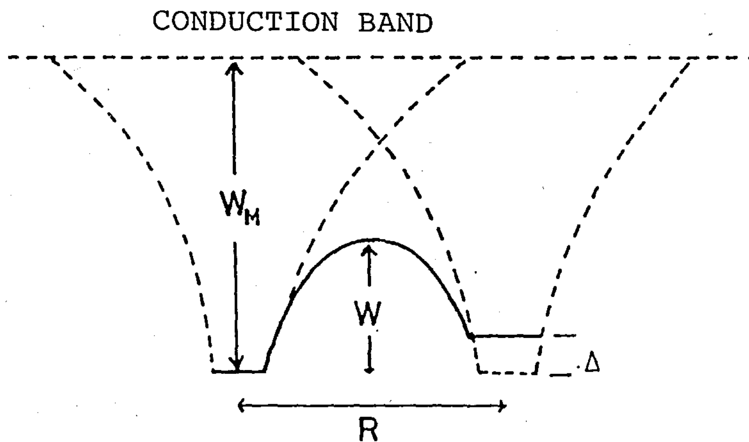

FIGURE (4) Model for overlapping Coulomblike potential wells for charged centers. The ground state energy is Wm, the potential separating these states is W, the potentials are centered a distance R apart, and the energy difference between two sites is denoted by Δ.

To calculate the a.c. conductivity, the effective relaxation time is taken to be

$$\tau \cong \tau_{oh} \exp (W/kT) \qquad (2.31)$$

where τ_{oh} being of the order of inverse Debye frequency. If we assume N states randomly and uniformly distributed in space and over an energy band Δo, with $g_o = N/\Delta o$, evaluation of the integrals proceeds in much the same way as in the tunneling case. The hopping distance for this case is obtained as

$$R\omega = \frac{e^2}{\pi \kappa [W_m + kT \ln (\omega \tau_{oh})]} \qquad (2.32)$$

which is a function of not the frequency alone, but the temperature as well.

To explain the frequency dependent conductivity in chalcogenides Elliot(25) introduced a new mechanism for hopping between two charged defect states. This mechanism arises when two electrons hop between states close to the Fermi level, but where the energy of the states is lowered after the arrival of electrons by relaxation of the lattice around them. The combined excitation is known as polaron, and for the two electrons hopping together, bipolaron(18).

The CBH of bipolarons has started from the suggestion that the effective correlation energy, U, at the defect centers becomes negative due to a strong electron-lattice interaction in chalcogenide glasses. Therefore existence of two polarons in one site becomes energetically favorable.

For the bipolaron hopping the CBH gives the a.c. conductivity as to a first-order approximation,

$$\sigma(\omega, T) = \frac{\pi^2 N^2 \kappa}{24} \left(\frac{8e^2}{\kappa W_m} \right)^6 \frac{\omega^s}{\tau_o^{1-s}} \qquad (2.33)$$

This equation predicts very different behavior from that expected for the QMT. If we use the same notation as before for frequency and temperature dependence, the frequency exponent s becomes temperature dependent, and if it is calculated in the form $[\partial \ln\sigma/\partial \ln\omega]_{T=const.}$, to a first order approximation to be

$$s = 1 - \frac{6kT}{W_m} . \tag{2.34}$$

s decreases from unity with increasing temperature. The decrease will be linear in temperature. The temperature dependence of $\sigma(\omega,T)$ for this case is frequency dependent. The slope of $\ln\sigma(\omega,T)$ versus T graph should be a constant.

The QMT and the CBH are the two basic models which are based on the pair approximation. Although there are further modifications to these models, such as taking the intrasite or intersite correlation energy into account, or introducing a limit to the extent of pair separation, R, and the like, the results are not so different(20), and they are beyond the scope of this study; and hence they will not be considered any further.

b. Unified Models-Extended Pair Approximation (EPA)

One of the basic assumptions of the above-mentioned theories is that the d.c. and a.c. components of the measured freqency dependent-conductivity are due to separable different mechanisms, because all of them are based on the pair approximation which deals only with the pure a.c. conductivity. However, the measured value includes a d.c. limit. Therefore, any interpretation which will be based upon a model derived from the pair approximation has to exclude the d.c. limit somehow from the measured quantities. Long suggests(20) that if the mechanisms responsible for a.c. conduction and d.c. conduction can be treated independently and

if the d.c. current is non-dispersive over the frequency spanned by the a.c. measurements then the observed conductivity can be written as

$$\sigma_T(\omega,T) = \sigma(0,T) + \sigma(\omega,T) \qquad (2.35)$$

where $\sigma(0,T)$ is the d.c. conductivity, and $\sigma(\omega,T)$ is the pure a.c. conductivity.

This approximation is hardly justifiable and has always been regarded with suspicion. In recent years there have been attempts to explain the frequency dependent conductivity in unified theories in which the same mechanisms are held responsible for both the non-dispersive low-frequency behavior and dispersive high-frequency response. While Movaghar et al.(26) tried to obtain this using an effective single particle random walk model, Summerfield and Butcher(27) have developed the Extended Pair Approximation (EPA) model. They consider both a.c. and d.c. behavior as due to interacting localized states within the framework of a model in which the pair approximation is applied to the network formalism of Miller and Abrahams(28), to which the ideas of percolation theory(29) can be applied for the d.c. limit.

The inputs to the EPA calculation of frequency dependent conductivity $\sigma(\omega,T)$ are transition rates and distribution of DOS around the Fermi level. $\sigma(\omega,T)$ for CBH and QMT type transition rates with four different DOS in the QMT model have been calculated(30)(31). The results, given in Figure (5), show that all curves are similar if they are plotted as $\ln[\sigma(\omega,T)/\sigma(0)]$ versus $\ln[\tilde{\omega}/\tilde{\sigma}(0)]$ where $\tilde{\sigma}(o) = \sigma(0)/g_o$, and $\tilde{\omega} = \omega/R_o$ with $g_o = e^2R_o/kT$, R_o being the rate parameter. The similarity between curves leads to a quasi-universal law in the form of:

$$\frac{\sigma(\omega)}{\sigma(0)} \simeq 1 + \left[A' \frac{e^2\omega}{kT\sigma(0)}\right]^n \qquad (2.35)$$

where n has been calculated to be around 0.725 and A' is a constant.

Summerfield's calculation reveals that the only difference

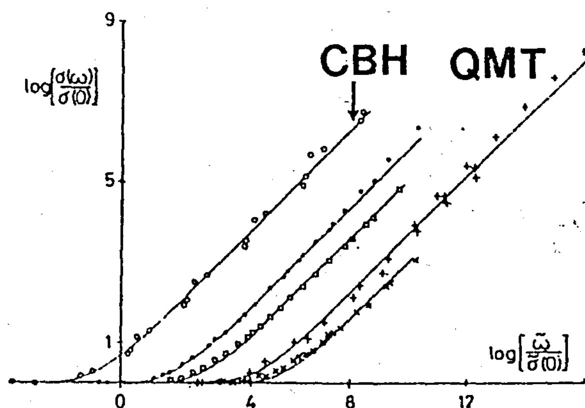

FIGURE (5) Scaled EPA conductivities for five models.

between the above-mentioned models is the difference in the numerical value of A'. Hence, a particular material has to be associated with a particular model in order to compare the experimental data with the numerical values of A'. Summerfield suggests that the association can be made by comparing the experimental d.c. values with the EPA predictions of dc conductivities for above mentioned models. On the other hand $A'=A\alpha$ and for hopping mechanisms that obey Mott's $T^{-1/4}$ law, the calculated EPA value for $A=1.1\times10^{-3}$. Hence using this value, it is possible to calculate the decay constant α. In fact, this is an alternative way to determining the three basic quantities $N(E_F)$, α, and the rate parameter R_o independently. Traditionally, the T_o and σ_o values are determined from the low temperature d.c. data by using Equation (2.1), provided data obey this law. Then, the $N(E_F)$, α, and R_o are calculated from Equations (2.2) and (2.3) by assuming a value for α. However, using a.c. data one can

independently determine the α value and then can evaluate the other parameters. This method is an alternative to 2-Dimensional hopping(32), field dependence of dc conductivity(33), and electron-spin resonance(34) methods in determining these three parameters independently.

EPA theory can also be tested using the d.c. values. In this limit, at low temperatures EPA calculations give(35), (36)

$$\sigma(0)_{EPA} = 1.34 \exp\left\{-1.33\,(T_0/T)^{1/4}\right\} \tag{2.36}$$

where $\sigma(o)_{EPA} = \sigma(o)/g_0\alpha$, $\sigma(o)$ being the measured d.c. conductivity, and

$$T_{0\,EPA} = \frac{24\,\alpha^3}{\pi N(E_F)k} \tag{2.37}$$

Equation (2.36) is in the form of Mott's Equation for variable range hopping (VRH) (Equation (2.1)), and it is a good approximation for VRH when

$$\left(\frac{T_0}{T}\right)^{1/4} \geq 10 \tag{2.38}$$

The EPA T_o can be determined from the experimental T_o' which in turn is determined from the slope of $\ln\sigma(o)$ versus $T^{-1/4}$ or $\ln(T\sigma(o))$ versus $T^{-1/4}$ graphs depending whether R_o is linearly dependent on temperature, T, (the former case) or whether R_o is independent of T (the latter case). Using the magnitude of the d.c. conductivity at a temperature T and the corresponding T_o, the pre-exponential factor σ_o is evaluated. By letting σ_o=1.34 $g_o\alpha$ and assuming a value for α (or calculating it from the a.c. data), one can either determine R_o/T, or R_o.

III. EXPERIMENTAL TECHNIQUES

A. Preparation of the Films

The amorphous silicon films and metal electrodes are evaporated in coplanar geometry on normal microscope slides of an area of 2.5x4.5 cm^2, produced by Fisher Scientific Co. The masks used in the evaporation process for silicon films and the metal electrodes are shown in Figure (6). The evaporation masks are made of aluminium metal plate of 0.55 mm thickness. Wires of 0.22 mm, 0.30 mm, and 0.37 mm diameters are placed in the rectangular space (1.5x2.5 cm^2) of the metal electrode masks to produce coplanar geometry.

Microscope slides are first cut to the desired dimensions and then cleaned with an alconox detergent in an ultrasonic vibrator. They are then rinsed with water. Aceton and methanol are used to remove the remaining grease and water vapor on the slides.

Two vacuum systems are used; one of which is an ion-pumped, and the other is a diffusion pumped type. In the former system the amorphous silicon films are evaporated and the latter is used for evaporation of metal (Aluminium) electrodes.

BOĞAZİÇİ ÜNİVERSİTESİ KÜTÜPHANESİ

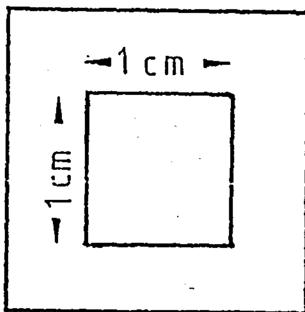

(a)

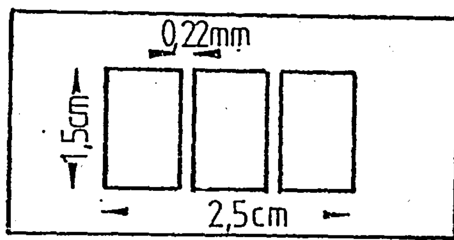

(b)

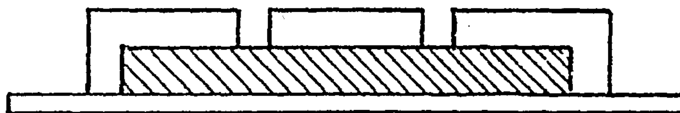

(c)

FIGURE (6) Masks used for obtaining amorphous silicon samples in coplanar geometry:

a) silicon mask,
b) electrode mask,
c) cross-section of the prepared sample.

The ion pumped vacuum system is pumped first down to 10^{-3} torr pressure with two cryopumps. In order to achieve lower pressures ion pumps are then used. The pumping time of the cryopumps is approximately one hour. Ion pumps operate continuously for 12 hours to drop the base pressure to 10^{-7}-10^{-8} torr. The pressure is measured with a thermocouple pressure gauge down to 10^{-3} torr and below that value with an ion gauge. The microscope slides (substrates) are placed on a substrate holder (Varian) on which three different masks can be prepared at a time.

The evaporation system used consits of an electron-gun and three crucibles produced by Varian. The position of the electron-gun can be adjusted by moving it with a system having bellows from outside without breaking the vacuum. The evaporant is a pure polycrystal lump obtained from Matheson Coleman and Bell laboratories. The distance between the evaporant and the glass substrates is 25 cm. This distance must be as long as possible in order to make the atoms to reach the surface of the films perpendicularly. Otherwise there will be hills and valleys on the surface of the film. To avoid impurity ion contamination the base pressure must be kept as low as possible. The base pressure is decreased to 10^{-8} torr before evaporation, while during the evaporation it is kept constant at pressures between $5\text{-}7 \times 10^{-7}$ torr. This is achieved by circulating liquid nitrogen through a jacket around the vacuum chamber.

The film thicknesses are between 3000-6000 Å. The evaporation of films takes about 3 hours. Evaporation rates in excess of ~ 1 Å/sec tend to produce films with high dark conductivities. After the deposition of the silicon films the vacuum system is allowed to cool in order to prevent formation of an oxide layer on the film. Then the system is opened and samples are taken out to the other evaporation system, for evaporating aluminium electrodes.

The-diffusion-pumped vacuum system has two vacuum pumps; one of which is a rotary pump for initial pumping (10^{-4} torr) and the other is a diffusion pump for lowering the pressure down to 10^{-6} torr level. In this vacuum system, pressure is measured by means of the Pirani and the Penning gauges.

Aluminium is thermally evaporated from tungsten filaments. During the evaporation the base pressure is kept around 10^{-4} torr. The thickness of the electrodes is around 1 μm and their evaporation takes about 2 mins. The thickness of the amorphous silicon films is measured by using optical interference techniques. A Sloan quartz crystal digital thickness monitor is used to adjust the evaporation rate. All of the samples used in this study are produced with the substrates at room temperature.

B. Experimental Setup

During the a.c. and d.c. measurements the samples are kept in two types of sample holder. For hot cycle, that is, for temperatures above room temperature a thermostatic chamber with temperature controllable to within ±1 degree throughout a range from -196°C to 600°C, is used. The pressure inside the chamber can be lowered to around 10^{-3} torr by a mechanical pump to avoid changes in conductivity due to water vapor condensation. The details of the chamber and sample holder is given in(37). We did not use this sample holder for cold cycles beause it consumes too much nitrogen as one goes to lower temperatures.

For cold cycles we used a very simple but efficient system consisting of a sample holder, a dewar, and a simple laboratory jack. Approximately 25 percent of volume of dewar is filled with liquid nitrogen. Using the temperature gradient in the dewar the temperature can be controlled to within ±0.5

degree. Since inside the dewar there is always nitrogen vapour which is heavier than air, the water vapour contamination risk is avoided. However, one should always go from high temperatures to low temperatures in the cold cycle; otherwise, since the sample holder is cooled to nearly 77 K when it is very close to the surface of the liquid nitrogen, as it is raised, to the top of the dewar, water vapor contamination cannot be prevented. Another point to be noted is that the rate of cooling increases when the sample holder comes closer to the surface of the liquid nitrogen.

C. D.C. Measurements

D.c. measurements include I-V measurements at room temperature and I-T measurements at constant electric field. The block diagram of the measurement system is given in Figure (7).

In order to take the I-V measurements the applied voltage is changed manually in 5-volt steps to achieve electric fields of 10^2 V/cm to 10^3 V/cm. The current for each setting is recorded after it stabilizes in order to avoid any capacitive effects. Applied voltage is measured with a digital voltmeter connected across the d.c. power supply so that the electrometer indicates the corect current passing through the sample. Since the internal resistance of the voltmeter is usually comparable with the sample resistance, it should not be connected parallel to the sample.

Contact photovoltage measurements were also performed by impinging a laser light onto the sample, and we have detected no current in the photodiode mode. I-V measurements showed that the I-V graph is symmetric for every sample measured, which taken together with the photovoltage measurements implies that the Al electrodes form an ohmic contact with the a-Si film(19).

A Philips PE 1520 type d.c. power supply, and two electrometers, one of which (a Cary 401 vibrating reed electrometer) is capable of measuring currents between 10^{-8} - 10^{-15} amperes, and other (a Keithley 614 digital type) beteween around 10^{-4} - 10^{-12} amperes were used in the measurements.

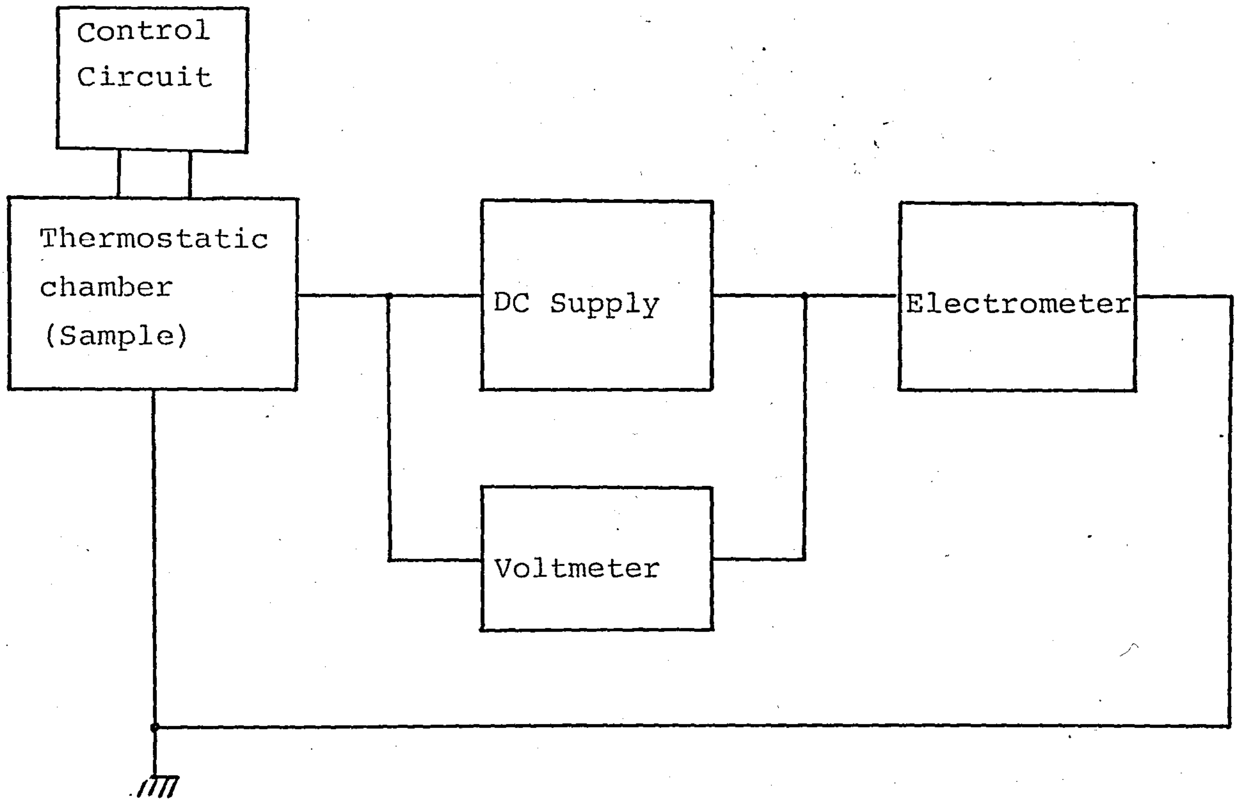

FIGURE (7) Block diagram of the d.c. measurement system.

D. A.C. Measurements

A.c. measurements include frequency dependence of conductance (G-f) measurements at constant temperature, and temperature dependence of conductance measurements (G-T) at constant frequency.

A.c. measurements were made at frequencies between 100 Hz and 2 MHz, and at temperatures between 150 K and 400 K. For a.c. measurements a Hewlett-Packard low-frequency

impedance analyzer LF 4192 A (5 Hz-13 MHz) was used. LF4192A is a vector-impedance meter and its accuracy is 0.1 percent in the frequency range used in our measurements. Measurements at frequencies higher than 2 MHz proved to be meaningless due to the inductance of the sample connection leads and stray capacitances.

Short and open offset adjustments were made before the measurements. All measurements were performed in the highest precision mode. Various admittances, formed by known capacitors and known high value resistors were connected in place of the sample and the capability of the measurement system was checked.

The peak value of the sinusoidal signal was kept at a level of 0.7 V-1.1 V, in order to measure the conductivity in the ohmic region.

The resistances of the films in coplanar samples are always much higher than the contact resistances and therefore we can be sure that the measured conductivities represent the sample properties.

The major difficulty encountered during the measurements is the environmental noise, which increases with the increase in sample resistivity as temperature is lowered. Thus, every connection was shielded, the circuit was grounded at only one point, and we avoided any movement that could cause some part of the circuit to vibrate.

Another problem in making G-T measurements is the discrepancy between the correct temperature of the sample and the one that is shown by the thermocouple. Since the thermocouples may heat/cool faster or slower than the sample, one should wait until the current reaches a steady value together with the thermocouple voltage.

Most of the problems have turned out to be due to bad

contacts. Therefore, in case of a problem in the measurement process, before trying anything, one should check every contact.

IV. EXPERIMENTAL RESULTS AND DISCUSSION

Figure (8) shows the pure a.c. conductiviy, $\sigma(\omega,T)$, versus temperature for one of the samples(38). The temperature dependence of the d.c. conductivity, $\sigma(0,T)$, is also shown in the figure. The d.c. conductivity has comparable values to a.c. conductivity only at high temperatures (roughly above 300 K) and is considerably smaller at low temperatures. Hence subtracting the d.c. term from the measured conductivity makes a difference only at high temperatures at which we can justifiably assume that the d.c. processes are due to band states or at least to the tail states.

Figure(9) shows the frequency dependence of $\sigma(\omega,T)$ at the indicated temperatures. In accordance with the data obtained by other researchers on evaporated amorphous silicon, our data also fit an empirical equation of the form

$$\sigma(\omega,T)=A\omega^{s} \qquad (4.1)$$

The exponent s is calculated from the slope of $\ln(\sigma(\omega,T))$ vs. $\ln(\omega)$ graphs.

In general s is around 0.6 at room temperature, decreases to 0.3 around 400 K, and increases to a value very

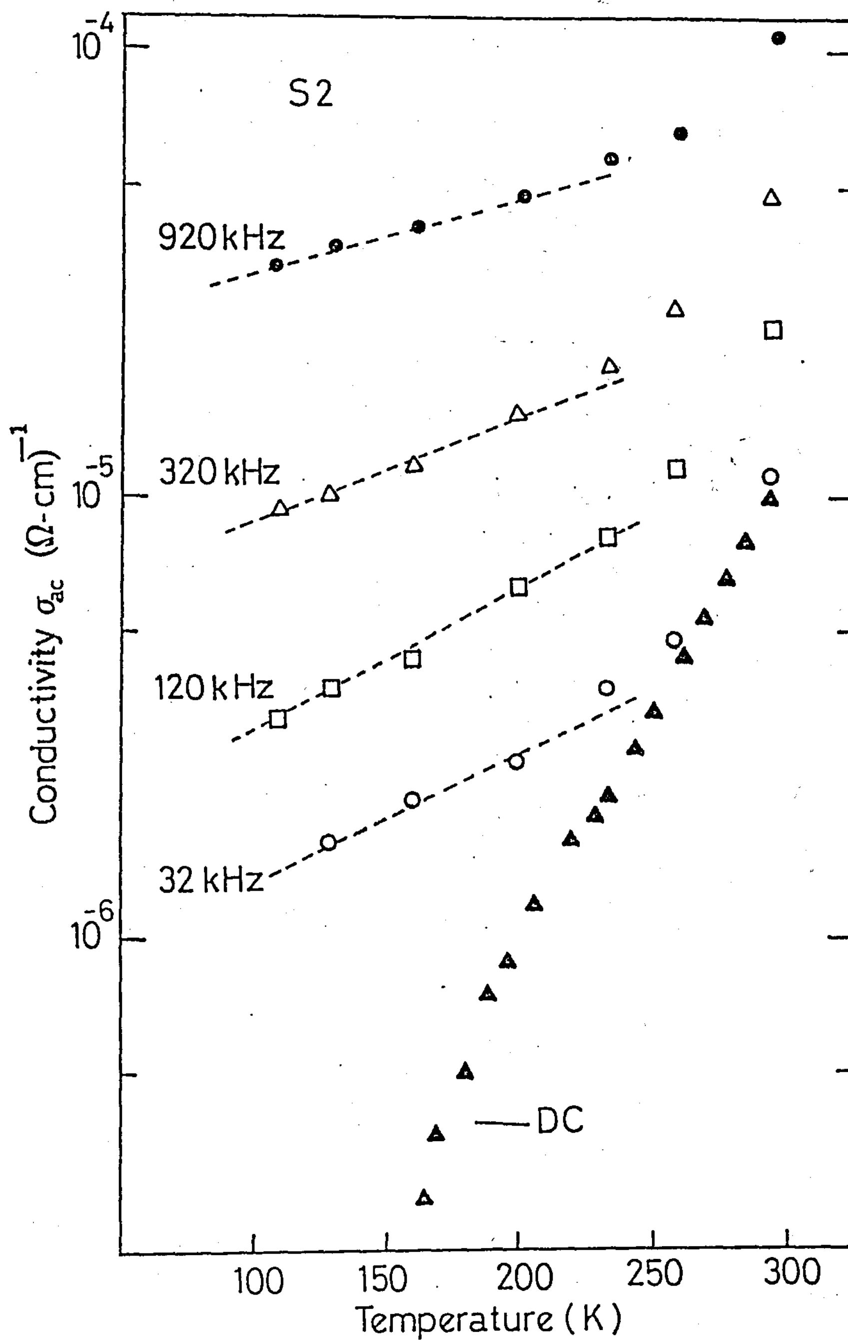

FIGURE (8) Temperature dependence of pure a.c. conductivity at the indicated frequencies, and d.c. conductivity of one of the samples. The dashed lines are drawn as a guide to eye for a linear relationship below 200K.

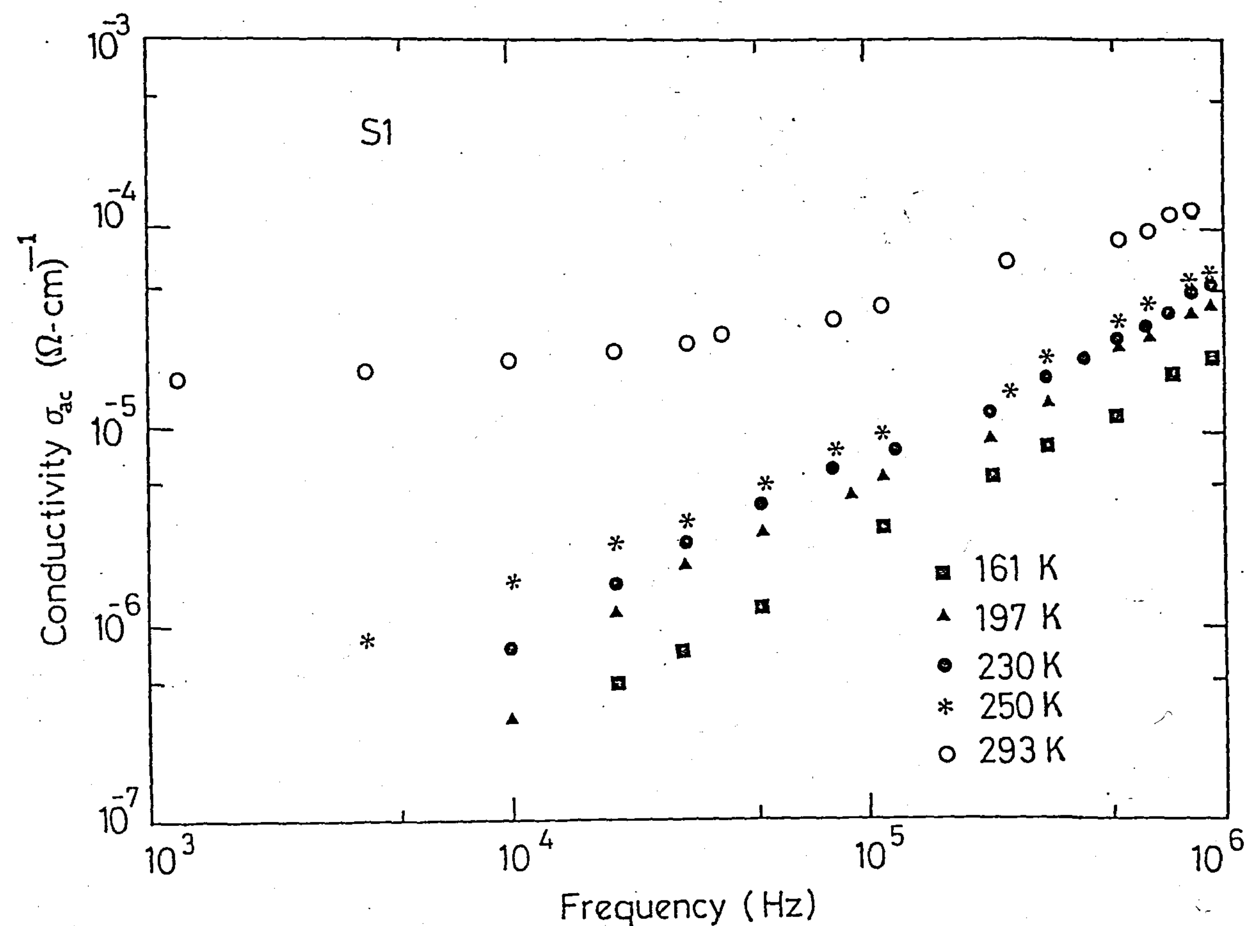

FIGURE (9) Frequency dependence of pure a.c. conductivity of one of the samples at indicated temperatures.

close to 1 around 150 K. Neither this behavior of s, nor the temperature dependence of $\sigma(\omega,T)$ is in agreement with the QMT model. This model predicts a linear dependence of conductivity on temperature and a temperature independent frequency exponent s with a constant value around 0.8.

In spite of the absence of non-bonding (lone-pair) orbitals in tetrahedrally bonded group IV amorphous semiconductors, Elliot(39) suggests the presence of spin-paired defects in amorphous silicon, concluding that as in the chalcogenide glasses, bipolaron hopping may be the predominant mechanism in amorphous silicon also. Therefore, we can apply the CBH model to our data.

Unlike the QMT model, the CBH model predicts a temperature dependent s which increases with decreasing temperature in agreement with our data. Table 1 gives the experimentally determined s values and those calculated according to Equation (2.34) at the indicated temperatures. In general, calculated and experimental s values approach each other around 250 K and the agreement between them gets better as the temperature decreases.

If s is taken to be around 0.95 at 192 K, Wm turns out to be 1.98 eV which is rather a large value considering that it is expected to be of the order of the optical band gap. However it should be emphasized that Wm has a very sensitive dependence on s. For example an s value of 0.93 at the same temperature gives Wm = 1.4 eV which is a more expected value. However it is very difficult to determine s so precisely within experimental error.

The temperature dependence can be seen more explicitly if Equation (2.33) is rewritten in the form

$$\sigma(\omega,T) = ab^{T/T_c} \qquad (4.2)$$

where $b=1/\omega\tau_o$, a stands for all other temperature independent parameters, and $T_c=Wm/6k$. Equation (4.2) can in turn be expressed as

$$\ln \sigma(\omega,T) = \ln a + \frac{T}{T_c} \ln b \qquad (4.3)$$

Since b and T_c are independent of temperature, the slope of $\ln(\sigma(\omega,T))$ versus T graph should be constant.

As can be seen from Figure(8) we can say that this is approximately the case below 200K. However, above 200K there is a stronger temperature dependence which can not be explained with the CBH model. A similar result was obtained by Reider who suggested that this discrepancy resulted from the fact that both Pike and Elliot considered only hopping between sites of equal energy(40). Taking into account an energy difference of Δ_o between the sites he came up with an a.c. conductivity in the form of

$$\sigma(\omega,T) \propto T \tanh(\Delta_o/2kT) \frac{\omega^s}{\tau_o^{1-s}} \qquad (4.4)$$

This is almost the same result obtained by Pike and Elliot but multiplied by $T\tanh(\Delta_o/2\ kT)$.

$\sigma(\omega,T)$ is calculated according to Equation (4.4) with the conductivity measured at the lowest temperature for each sample used as a scaling factor. The results are given in Table 1. Once again the agreement between theory and experiment is better at lower temperatures. The stronger temperature dependence observed above 200 K cannot be explained by Reider's theory either.

Long has suggested that the a.c. conductivity in evaporated a-Si films could be explained by a Polaron Tunneling Model in which an electron tunnels between states

Sample No	Temp. (K)	s_{meas}	$s_{calc.}$	$\sigma(\omega,T)$ measured $(\Omega\text{-cm})^{-1}$	$\sigma(\omega,T)$ calculated $(\Omega\text{-cm})^{-1}$
	161	0.97	0.93	8.82×10^{-7}	....
	197	0.94	0.92	2.00×10^{-6}	2.26×10^{-6}
S1	230	0.88	0.90	2.50×10^{-6}	2.00×10^{-6}
	250	0.85	0.89	3.33×10^{-6}	2.54×10^{-6}
	293	0.48	0.87	2.67×10^{-5}	4.05×10^{-6}
	198	0.96	0.91	2.47×10^{-6}	....
S2	231	0.90	0.90	3.67×10^{-6}	3.36×10^{-6}
	256	0.86	0.89	4.75×10^{-6}	4.34×10^{-6}
	292	0.75	0.87	1.10×10^{-5}	6.74×10^{-6}
	190	0.97	0.92	1.28×10^{-6}	....
S3	211	0.85	0.91	1.83×10^{-6}	1.66×10^{-6}
	273	0.76	0.88	3.72×10^{-6}	3.41×10^{-6}
	293	0.71	0.87	6.81×10^{-6}	4.27×10^{-6}
	192	0.99	0.92	1.30×10^{-7}	....
	233	0.84	0.90	3.30×10^{-7}	2.15×10^{-7}
S4	297	0.64	0.87	2.20×10^{-6}	4.35×10^{-7}
	321	0.60	0.86	4.20×10^{-6}	5.49×10^{-7}
	342	0.45	0.85	9.20×10^{-6}	6.82×10^{-7}
	186	0.90	0.92	1.65×10^{-6}	....
	223	0.83	0.90	2.95×10^{-6}	2.69×10^{-6}
	239	0.67	0.90	4.02×10^{-6}	2.88×10^{-6}
S5	256	0.60	0.89	4.42×10^{-6}	3.60×10^{-6}
	266	0.68	0.89	5.36×10^{-6}	3.74×10^{-6}
	291	0.59	0.87	2.75×10^{-5}	5.57×10^{-6}

TABLE 1. Experimentally determined a.c. conductivities and s values and those calculated according to Equations (2.34) and (4.4) at 32 kHz. For each sample $\sigma(\omega,T)$ value measured at the lowest temperature is used to scale the other calculated $\sigma(\omega,T)$ values. The parameters used in the calculations are W_m=1,2 eV, $\tau_o=10^{-12}$ sec, Δ_o=0.1 eV, and κ=3.

close to the Fermi energy, E_F, and the energy of the states is lowered after the arrival of the electron due to the lattice distortion(20). The relaxation time for polaron tunneling at relatively high temperatures is given by

$$\tau = \tau_p \exp (W_H/kT) \exp (2\alpha R_\omega) \tag{4.5}$$

where τ_p is of the order of the optical phonon frequency, R_ω is the tunneling distance, and W_H is the hopping activation energy. For large polarons

$$W_H = W_o (1 - \frac{r_o}{R_\omega}) \tag{4.6}$$

where W_o is the maximum activation energy, and r_o is the polaron radius. The a.c. conductivity and the frequency exponent s are given as:

$$\sigma(\omega,T) = \frac{\pi^4}{12} (N_f kT)^2 e^2 \frac{\omega \quad R_\omega^4}{(2\alpha kT + \frac{W_o r_o}{R_\omega^2})} ; \tag{4.7}$$

if Equation (4.7) is expressed in the form of Equation (4.1) then,

$$s = 1 - \frac{4 + 6(\beta W_o r'_o / R'^2_\omega)}{R'_\omega [1 + (\beta W_o r'_o / R'^2_\omega)]^2} \tag{4.8}$$

where $\beta = 1/kT$, $r'_o = 2\alpha r_o$, $R'_\omega = 2\alpha R_\omega$. The optimum hopping length is calculated from

$$R'^2_\omega + [\beta W_o + \ln(\omega \tau_p)] R'_\omega + \beta W_o r'_o = 0 . \tag{4.9}$$

s values calculated from the experimental data are plotted against temperature in Figure (10). As we have indicated earlier s is a decreasing function of temperature

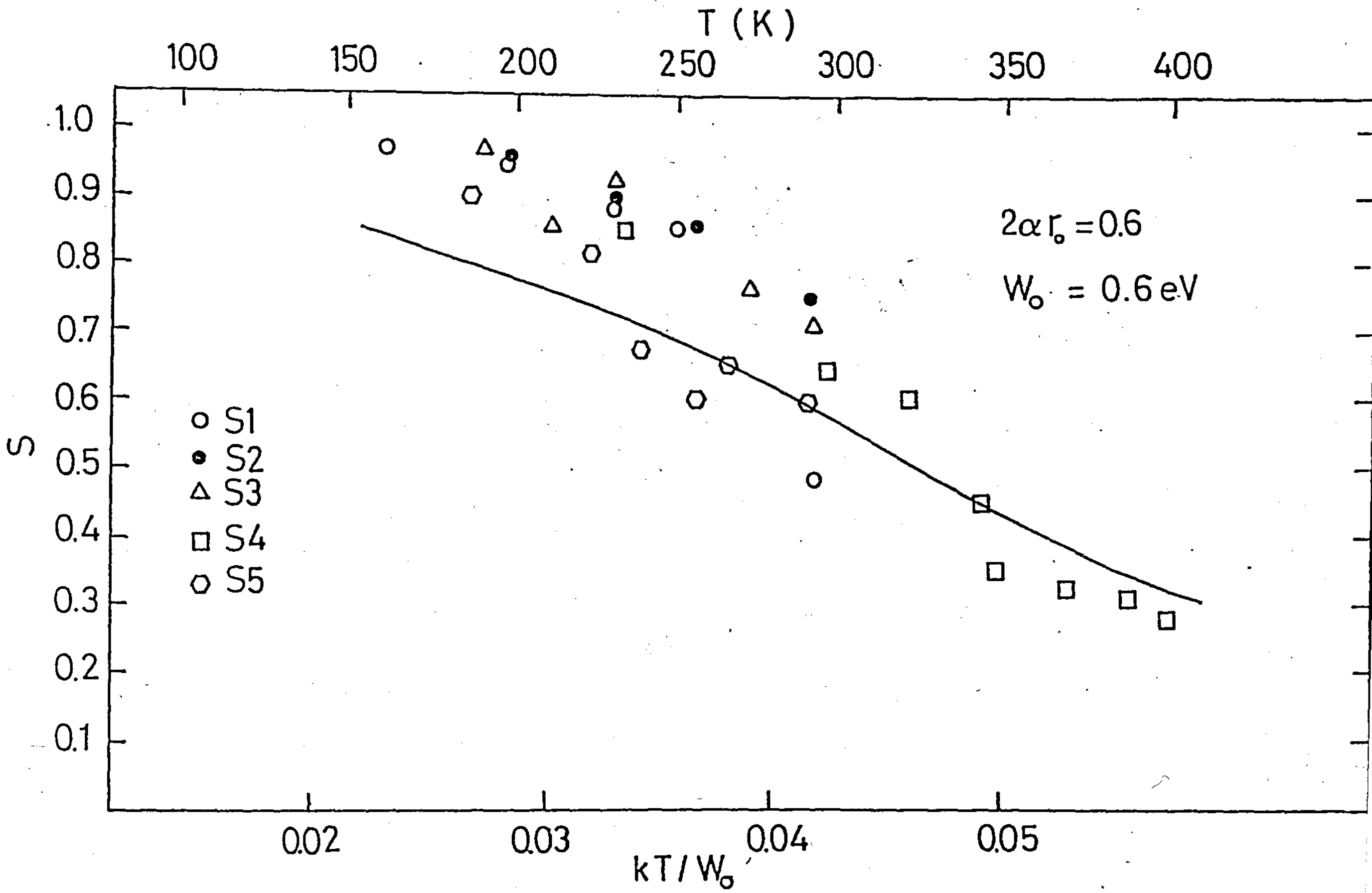

FIGURE (10) s-values plotted against temperature scaled to the large polaron activation energy. The line is calculated from the polaron tunneling model for W_o = 0.6 eV, and $2\alpha r_o$ = 0.6, $\tau_p = 10^{-12}s$, and f = 32 kHz.

but the dependence is not linear as the CBH suggests. The solid line represents the best fit of Equation (4.8) to the experimental data with $\tau_p=10^{-12}$ s, f=32 kHz, r_o and W_o values, determined in trying to find the best fit to the data, are 3 A^o and 0.6 eV respectively assuming that α^{-1}=10 A^o.

The theory suggests a minimum at higher temperatures but since our data do not reach these temperatures we have no way of commenting on this feature of the model. Such a minimum has been observed for a-Ge at 400 K(20), whereas Shimakawa's results on a-Si:H reveal no such minimum up to 300 K(41). The best fit also yields a DOS around the Fermi level, $N(E_F)=2\times10^{23}$ $(cm^3\text{-}eV)^{-1}$, at T=230 K and f=32 kHz with $\sigma(\omega,T)=2.4\times10^{-6}$ $(\Omega\text{-cm})^{-1}$, which is a rather high value.

Figure (11) shows the d.c. conductivities for four samples as plotted against T^{-1}. In the high temperature range the activation energies of all the samples are of the order of 0.3 eV. This indicates a conduction mechanism in the tail states. As the temperature decreases the activation energies of the samples decrease as well. Figure (12) shows the d.c. conductivities as plotted against $T^{-1/4}$. All samples obey $T^{-1/4}$ law in a temperature range of 77-200 K. Hence, we can apply the EPA results for the QMT in this temperature region.

Figures (13) and (14) shows the graphs of $\ln[\sigma(\omega,T)/\sigma(0)]$ versus $\ln[e^2\omega/kT\sigma(0)]$ for the indicated samples. The dotted lines in both graphs represent the best fit of the data to Equation (2.35). The average n and A' values, calculated from the best fit, are 0.69±0.05 and $9.88\times10^6\pm1.18\times10^7$ cm^{-1} respectively. In fact for the samples 1,3,4, and 5 the average $A'=4.00\times10^6\pm1.91\times10^6$ cm^{-1}. We have found no explanation for the A' value of sample 2 which is 3.33×10^7. The α^{-1} value calculated from the average A' value and the EPA A result given above is 1.1×10^{-2} Å which is an unacceptably small value.

If on the other hand one uses the EPA A value for the

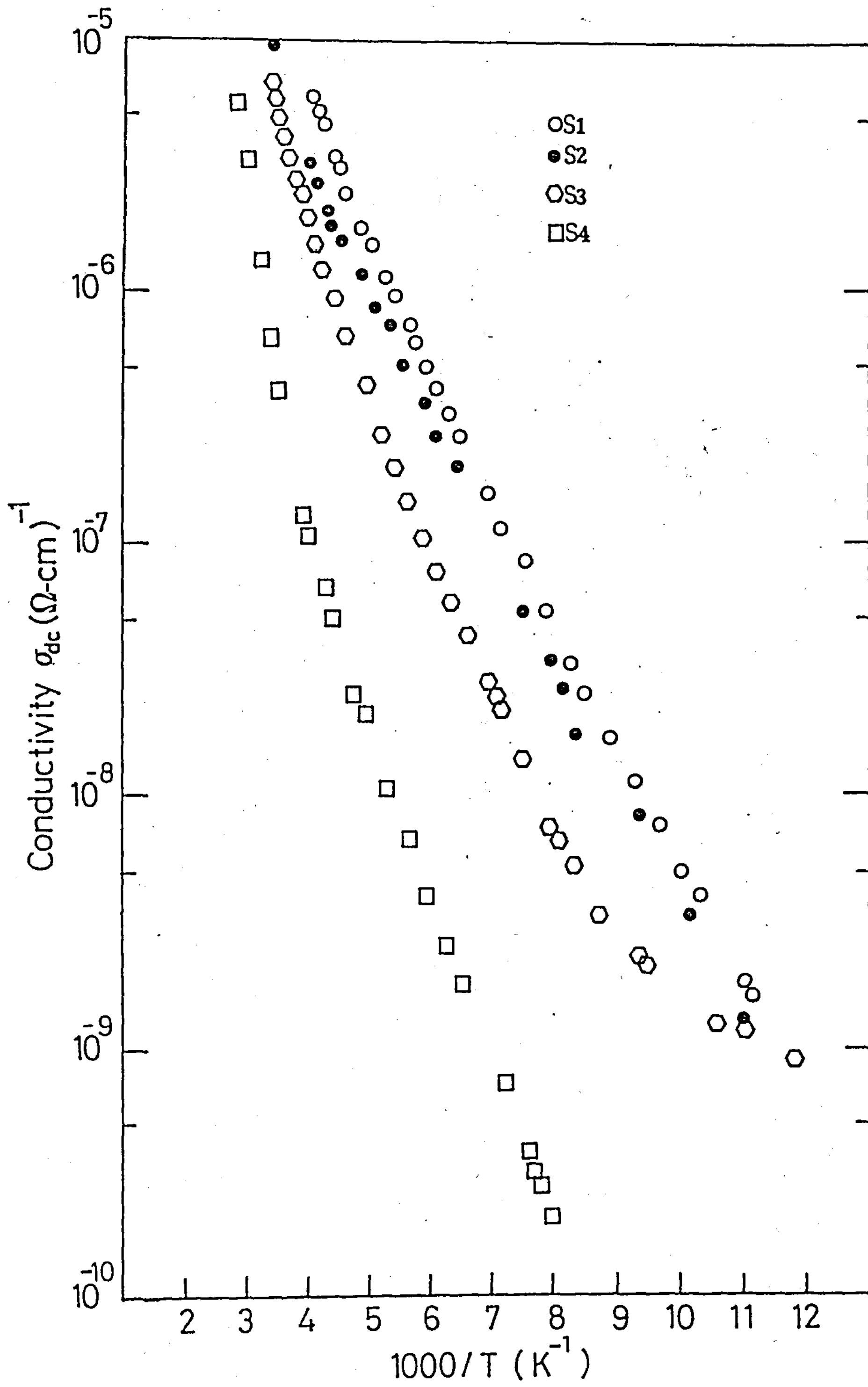

FIGURE (11) Inverse temperature dependence of d.c. conductivities for four samples.

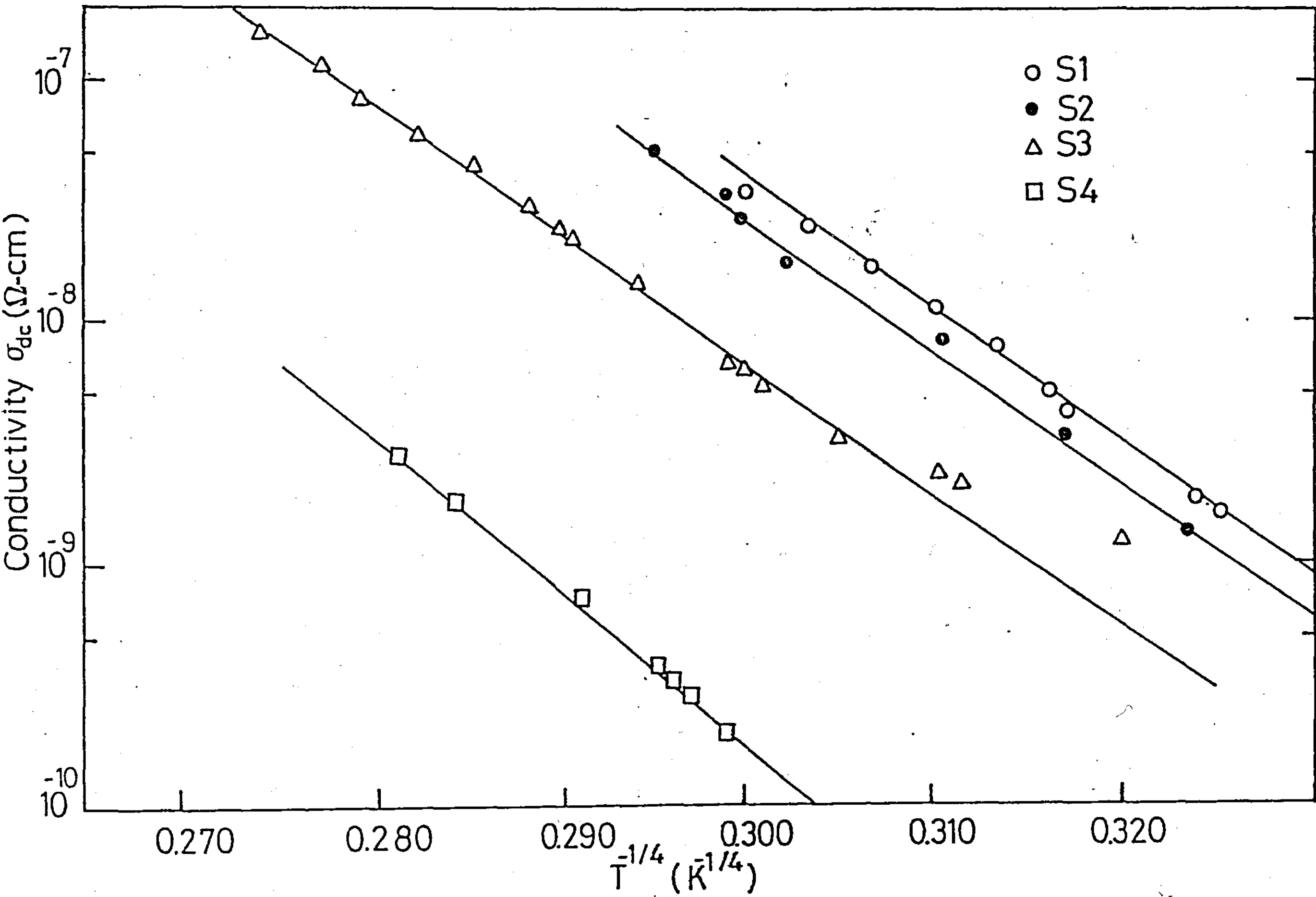

FIGURE (12) D.c. conductivities of four samples as plotted against $T^{-1/4}$.

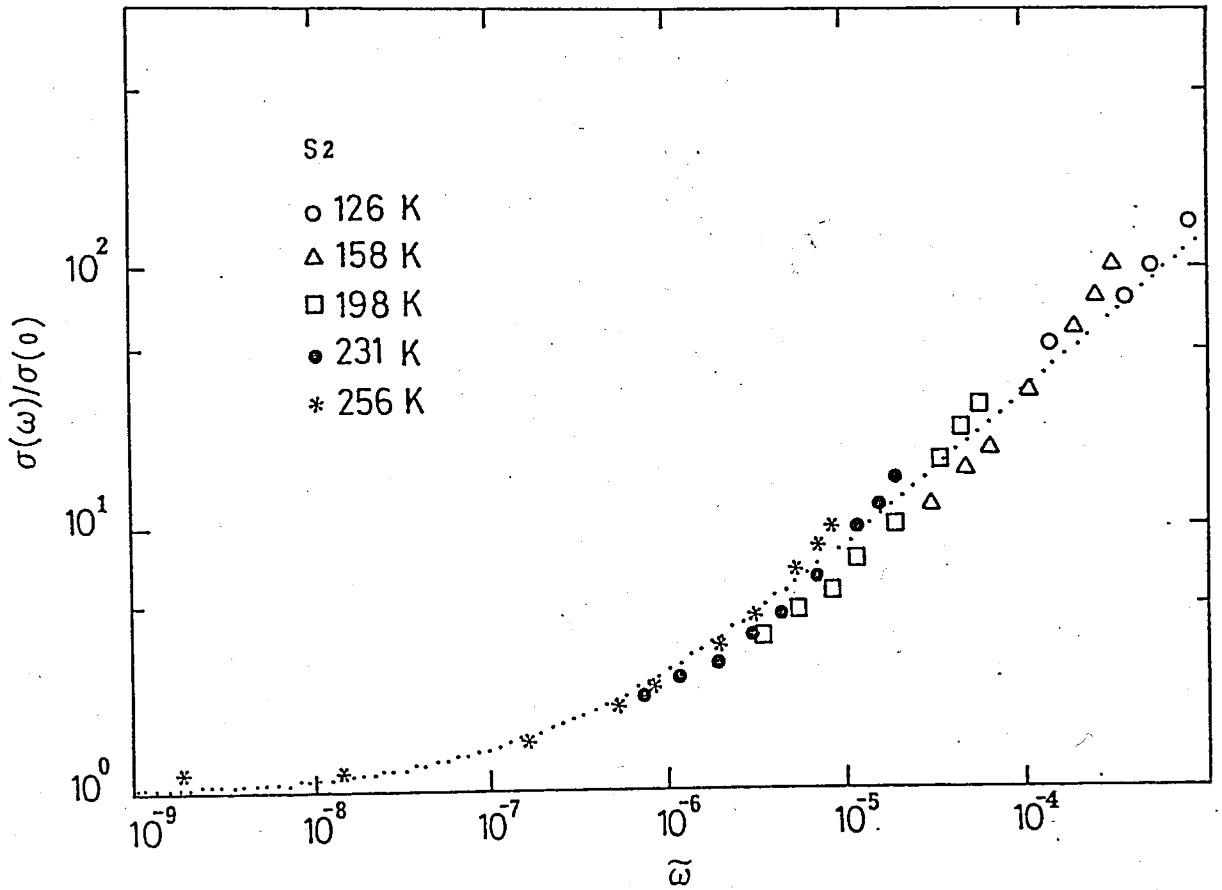

FIGURE (13) Reduced frequency-dependent conductivity against reduced frequency for sample-2.

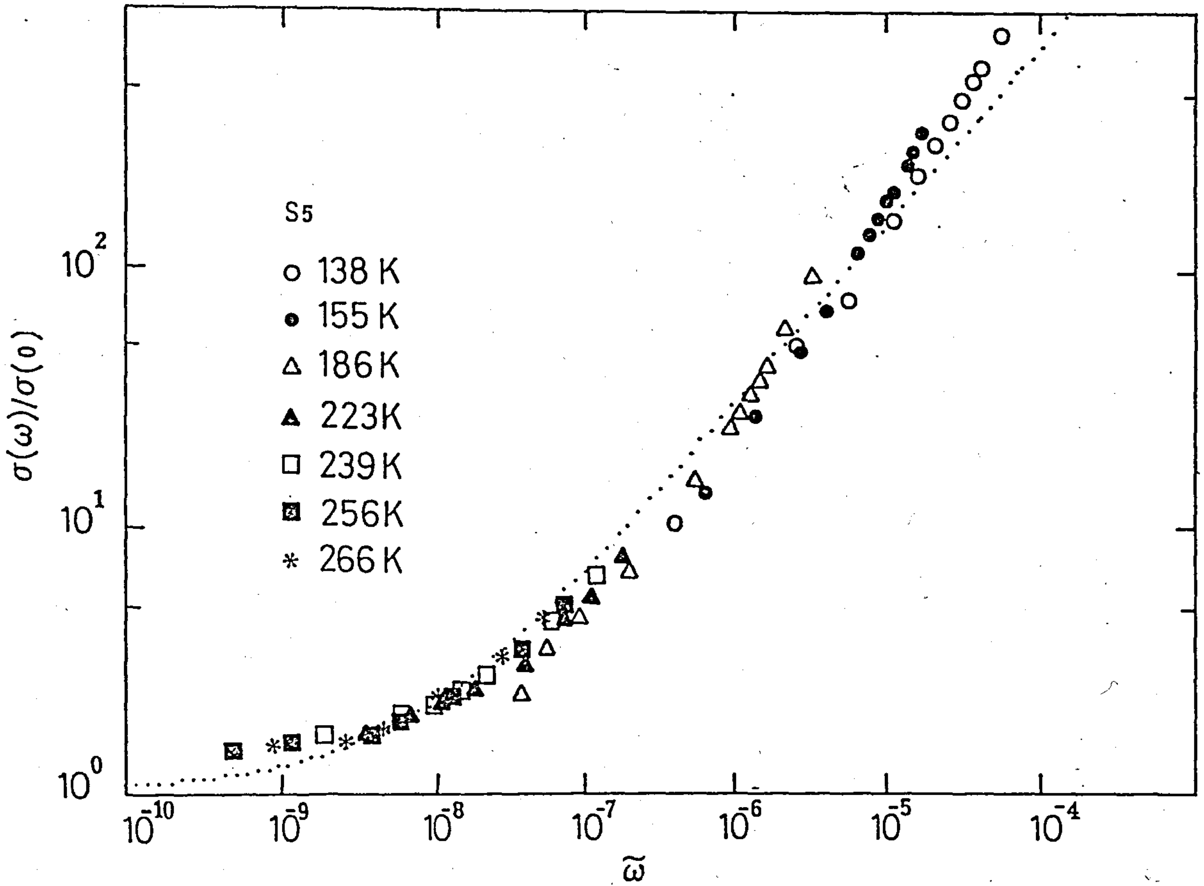

FIGURE (14) Reduced frequency-dependent conductivity against reduced frequency for sample-5.

CBH which is 5.37 the average α^{-1} value is obtained as 136 Å , which is rather a high value. In Table-II the α^{-1} values calculated using the CBH results are also given.

We have tested EPA theories using the d.c. values also. In this limit, at low temperatures, the EPA results are given in Table 2. Since most of the a.c. data produced an unacceptable value for α, in all the d.c. calculations α^{-1} is taken to be 10 Å .

The results obtained for the rate parameter R_o in energy dependent and independent cases are very high if we consider that R_o is expected to be of the order of the phonon frequency, $\sim 10^{12}$-10^{13} Hz(42).

The $N(E_F)$ values of $\sim 10^{18}$ $(cm^3\text{-}eV)^{-1}$ calculated from Equation (2.37) with EPA T_o values are slightly low by comparison with what is expected for evaporated a-Si, which is of the order of 5×10^{19} $(cm^3\text{-}eV)^{-1}$(43),(44).

The fact that a.c. results fit perfectly the quasi-universal law predicted by this model is indicative that the d.c. and a.c. conductions are due to the same mechanisms. However the quantitative parameters derived from a comparison of the data with the model are not as satisfactory.

Sample No	Temperature	$\sigma(0)$	T_{0EXP}	T_{0EPA}	R_0/T	T_{0EXP}	T_{0EPA}	R_0	$N(E_F)$	α^{-1}
			$R_0 \propto T$			R_0 independent of T				Calculated from the CBH transition rates
S1	89	1.60	2.63	8.42	6.33	3.83	1.23	3.89	1.05	225
S2	91	1.35	2.48	7.94	2.36	3.76	1.20	1.96	1.12	16
S3	116	4.30	2.32	7.42	0.386	3.56	1.14	0.275	1.19	113
S4	125	2.00	4.48	14.3	0.624	6.31	2.02	3.15	0.620	250
S5	86	3.50	2.08	6.66	0.198	2.73	0.874	0.0319	1.33	79
		$\times 10^7$	$\times 10^8$	$\times 10^7$	$\times 10^{16}$	$\times 10^8$	$\times 10^8$	$\times 10^{18}$	$\times 10^{18}$	
Unit	K	Sm^{-1}	K	K	$(secK)^{-1}$	K	K	sec^{-1}	$(cm^3\text{-}eV)^{-1}$	Å

TABLE 2. The EPA d.c. results. α^{-1} is taken to be 10 Å in the calculations.

V. CHARACTERIZATION OF AMORPHOUS SEMICONDUCTORS BY PHOTOCONDUCTIVITY MEASUREMENTS

A. Phase Shift Analysis of Modulated Photocurrent (PSAMP) Method

The PSAMP method has recently been successfully used to determine the density of states (DOS) distribution in the energy gap of amorphous semiconductors(6),(8),(9),(10),(45),(46). In this method, a sinusoidally modulated excitation light is used and a phase shift is observed between this excitation light and the induced photocurrent. The phase shift and the amplitude of the photocurrent observed at a particular modulation frequency ω and temperature T are closely related to the density of states M(E) at a particular energy level E. In this analysis an energy level scheme shown in Figure (15) is considered.

The rate equations for the generation of an electron into the conduction band and for an electron trapped at a localized state with an energy E_d below the conduction band are expressed, respectively, as

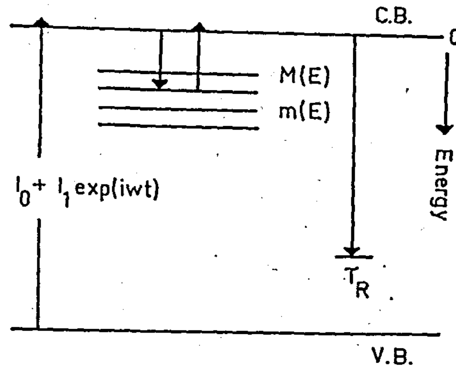

FIGURE (15) Energy level scheme for the analysis of the PSAMP method.

$$\frac{dn}{dt} = I_o + I_1 \exp(i\omega t) - \int_0^{E_d} \frac{dm(E)}{dt} dE - \frac{n - n_d}{\tau_R} \qquad (5.1)$$

$$\frac{dm(E)}{dt} = n(M(E) - m(E))\nu\sigma - N_c \nu\sigma M(E) \exp(-E/kT) \qquad (5.2)$$

where n is the concentrations of electrons in the conduction band, n_d the value of n in the dark, m(E) the number of trapped electrons in the localized gap states with a density M(E), E_d the electron demarcation level, τ_R the recombination time for electrons and holes in the conduction and valence bands, respectively, ν the thermal velocity, σ the capture cross-section for an electron, N_c the effective density of states in the conduction band, and ω the frequency of the exciting light and the modulated photocurrent. It is here assumed that the capture cross section σ is independent of energy and temperature and that there is only one type of tail state.

The solutions of the rate equations are expected to have the following forms:

$$n = n_o + n_1 \exp(i\omega t) \qquad (5.3)$$

$$m(E) = m_o(E) + m_1(E) \exp(i\omega t) \qquad (5.4)$$

Using these expressions, the rate equations (5.1) and (5.2) can be solved exactly, and one obtains

$$\tan\phi = \frac{\omega + \frac{\pi}{2} kT\sigma\nu M(E_\omega)}{\frac{1}{\tau_R} + \int_0^{E_{fn}} \nu\sigma M(E)\, dE} \qquad (5.5)$$

for the phase angle ϕ between the excitation light and the induced photocurrent(6). Here E_{fn} is the quasi-Fermi level. The energy that corresponds to each value of the density of states can be calculated using the expression

$$E = kT \ln\left(\frac{N_c \nu\sigma}{\omega}\right) \qquad (5.6)$$

and is measured from the edge of the conduction band. Assuming the $N_c\nu\sigma$ is independent of energy, the energy scale can be scanned from the bottom of the conduction band to the Fermi level by varying the modulation frequency and temperature.

Since the phase angle ϕ_j and the modulated photocurrent I_j are measured as a function of modulation frequency in the experiment, it will be better to express the denominator in Equation (5.5) as a sum. Hence,

$$A = \frac{1}{\tau_R} + \int_{E_1}^{E_{fn}} \sigma\nu M(E)\, dE + \int_{E_j}^{E_1} \sigma\nu M(E)\, dE \qquad (5.7)$$

$$\Lambda = \frac{1}{\tau_{RO}} + \sum_{s=2}^{j} kT \ln \frac{\omega_s}{\omega_{s-1}} \sigma\nu M(E_{s-1}) \qquad j=2,\ldots,N \tag{5.8}$$

where

$$\frac{1}{\tau_{RO}} = \frac{1}{\tau_R} + \int_{E_1}^{E_{fn}} \sigma\nu M(E)\, dE \tag{5.9}$$

Unless M(E) doesn't assume a very low value, τ_{RO} becomes very small and one can neglect $\tau_{RO}\omega$ term in Equation (5.5). By using Equations (5.5)-(5.8) one obtains the working equations (47),

$$\tau_{RO}\sigma\nu M(E_1) = \frac{2}{\pi kT} \tan\phi_1 \tag{5.10}$$

$$\tau_{RO}\sigma\nu M(E_j) = \frac{2}{\pi kT} \left[1 + \sum_{s=2}^{j} kT \ln \frac{\omega_s}{\omega_{s-1}} \sigma\nu\tau_{RO} M(E_{s-1}) \right] \tan\phi_j \tag{5.11}$$

where $j=2,\ldots,N$. Equations (5.10) and (5.11) are the basic relations in determining the DOS distribution.

Aside from the phase angle between the excitation light and the induced photocurrent, the magnitude of the photocurrent is also measured during the experiment. Theoretically, the expression for the photocurrent is given as

$$I_{ac} = \frac{\tau_{RO} C}{\left\{ \left[1 + kT \sum_{s=2}^{j} \ln \frac{\omega_s}{\omega_{s-1}} \tau_{RO} \nu\sigma M(E_{s-1}) \right]^2 + \left[\pi kT \tau_{RO} \nu\sigma M(E_j) \right]^2 \right\}^{1/2}} \tag{5.12}$$

where $j=2,3,4,\ldots,$ and C depends on experimental conditions, and must be kept constant during a set of frequency measurements at a constant temperature ,T. The theoretical magnitude of the modulated photocurent is calculated using Equations (5.6), (5.10), (5.11), (5.12) and normalized to the value at ω_1. This value is compared with the normalized, experiment-

ally masured values of the current. If the difference between these values is negligible, this method can be seen to be self-consistent and its validity is further assured.

As can be seen from Equation (5.6) w corresponds to the thermal emission rate of a trapped electron at the energy level E.

In the experimental procedure, the modulation frequency is varied at a constant temperature, and the phase shift values are determined at each frequency. This is then repeated for other temperature values. Since according to (5.6) an energy level specified with ω_1 at temperature T_1 can also be obtained with ω_2 at temperature T_2, the phase shift spectra of each temperature will represent partly overlapping sections of the same density of state distribution. These overlapping regions and the exact position of an energy level E cannot be determined exactly unless the value of the product $N_c \nu \sigma$ is known.

When analyzing the experimental results, one of the major problems is the determination of these overlapping regions and the exact position of an energy level E. This product up to now has been determined by two methods, one of which depends on the existence of a characteristic peak present in the DOS profile of each temperature(6),(9),(10) and the other of which involves calculations utilizing the intensity of the modulated photocurrent in addition to the phase angle(48).

In the first method the observed peak will shift to higher frequencies as the temperature is increased. A plot of peak frequency versus temperature yields the activation energy corresponding to the energy position of the localized level associated with the peak. This value is then used to determine the energy axis of the DOS distribution. However, the characteristic peak may not exist at all(8),(45) or even if it does, it is only when the peak is very sharp that

it is possible to determine the frequencies at which it exists. In this case different temperature-frequency combinations corresponding to the same energy can be used to determine the overlapping regions of phase spectra of different temperatures, but both these calculations and the energy axis will be arbitrary to the extent of the assumption made for the value of $N_c\nu\sigma$.

This arbitrariness can be avoided if the intensity of the photocurrent is used in addition to the phase shift values in the determination of both DOS and the corresponding energy position(48). But this case can only be applied to measurements in which the experimental conditions have been kept constant throughout the whole experiment. This is difficult to do. We presented an alternative solution to determine $N_c\nu\sigma$ even when the experimental conditions are not kept constant(11).

B. A New Approach to Determining the Energy Scale(11)

The phase shift ϕ_{nj} at the modulated frequency w_j and temperature T_n is given by Equation (5.5), as

$$\tan \phi_{nj} = \frac{B_{nj}}{A_{nj}} \tag{5.13}$$

where

$$B_{nj} = \omega_j + \pi k T_n \nu\sigma M(E_{nj}) \tag{5.14}$$

$$A_{nj} = \frac{1}{\tau_{R0}} + \int_{E_{nj}}^{E_i} \nu\sigma M(E)dE \tag{5.15}$$

The intensity of the photocurrent at the modulation frequency ω_j and temperature T_n can be expressed as

$$I_{nj} = \frac{C_n}{(A_{nj}^2 + B_{nj}^2)^{1/2}} \tag{5.16}$$

by using Equations (5.12), (5.14), and (5.15). Here C_n depends on experimental conditions. According to Equations (5.13) and (5.16), by considering the triangle

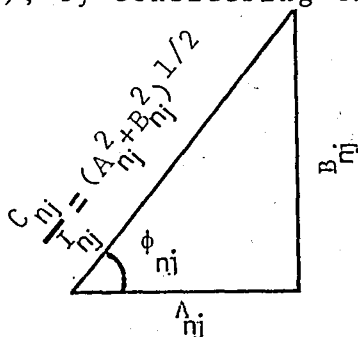

we can define the following quantities

$$\alpha_{nj} = \frac{\cos \phi_{nj}}{I_{nj}} = \frac{A_{nj}}{C_n} \tag{5.17}$$

$$\beta_{nj} = \frac{\sin \phi_{nj}}{I_{nj}} = \frac{B_{nj}}{C_n} \tag{5.18}$$

and

$$\gamma_{nj} = \frac{\tan \phi_{nj}}{T_n} = \frac{B_{nj}}{A_{nj}\, T_n} \tag{5.19}$$

If we neglect the ω_j term in Equation (5.14), $M(E_{nj})$ is obtained using Equation (5.11) as

$$M(E_{nj}) = \frac{N_c C_n}{N_c v \sigma} \frac{\beta_{nj}}{\pi k T_n} \tag{5.20}$$

and the energy level E_{nj} is determined from Equation (5.6).

In order to obtain $N_c\nu\sigma$ we may equate different frequency-temperature combinations corresponding to the same energy, $E(\omega_p,T_1) = E(\omega_q,T_2)$, to obtain

$$\ln(N_c\nu\sigma) = \frac{T_2}{T_2 - T_1}\ln\omega_q - \frac{T_1}{T_2 - T_1}\ln\omega_p \tag{5.21}$$

The major problem here is to find an ω_q value from among the frequency values of temperature T_2 that satisfies the above relation for an arbitrarily chosen ω_p value at temperature T_1.

In the case of constant Cn's throughout the experiment, calculated α_{nj} values can be used(48). However, if Cn's differ for different temperature data sets we have to make use of γ_{nj} values instead. From (5.14), (5.17), (5.18), and (5.19), γ_{1p} and γ_{2q} corresponding to (ω_p,T_1) and (ω_q,T_2) respectively are given by

$$\gamma_{1p} = \frac{\pi k\nu\sigma M(E_{1p})}{A_{1p}} \tag{5.22}$$

$$\gamma_{2q} = \frac{\pi k\nu\sigma M(E_{2q})}{A_{2q}} \tag{5.23}$$

Then, according to (5.15), $A_{1p} = A_{2q}$ and, since $E(\omega_p,T_1) = E(\omega_q,T_2)$, $\gamma_{1p} = \gamma_{2q}$. Another way of expressing this is

$$\frac{\tan\phi_{1p}}{T_1} = \frac{\tan\phi_{2q}}{T_2}\ . \tag{5.24}$$

At a temperature T_1 an ω_{1P} is chosen arbitrarily. The phase shift ϕ_{1p} corresponding to this ω_{1P} and T_1 is used to determine γ_{1p}. This value is found among the γ values calculated from the data taken at another temperature T_2. Then the phase shift ϕ_{2q} and hence the corresponding ω_{2q} are

determined. This frequency ω_{2q} together with ω_{1p}, T_1, and T_2 values are used in Equation (5.21) to calculate $N_c\nu\sigma$. This value now can be used in Equation (5.6) to determine the energy levels E_{nj}. The corresponding $M(E_{1j})$ values given in Equation (5.20) are also calculated using this value. $N_c C_1$ is chosen arbitrarily. $M(E_{nj})$ values with n=2,3,... are then determined by normalizing each C_n with respect to C_1. The normalization factor, according to Equation (5.17), is given by

$$\frac{\alpha_{1p}}{\alpha_{nq}} = \frac{C_n}{C_1} \qquad (5.25)$$

In order to illustrate this procedure, "data" generated from a hypothetical DOS distribution, given in Figure (16), are used. For temperatures of 300, 320, 340, 360, 380, and 400 K, ϕ_{nj} and I_{nj} values corresponding to frequencies of 50-2000 Hz using Equations (5.6), (5.13)-(5.16) are shown in Figure (17) and Figure (18). The parameters employed in the calculations are $N_c\nu\sigma = 10^{-10} s^{-1}$, and $(\tau_{RO}\sigma\nu)^{-1} = 6\times10^{6}$ cm^{-3}. These values were determined in the process of finding the best fit to the original curve. The photocurrent values of Figure (18) are normalized with respect to the smallest photocurrent value which is arbitrarily taken to be 0.1.

Here we only give the results obtained from the data generated that are relevant for explaining the above procedure. Figure (19) represents the determination of $N_c\nu\sigma$ graphically. The solid line represents Equation (5.21) with ω_p=70 Hz, T_1=300 K, and T_2=320 K. The dashed lines represent (a) γ_{1p} corresponding to 70 Hz, (b) the equivalent γ_{2q}, (c) the equivalent ω_q, and (d) the corresponding value of $N_c\nu\sigma$, 10^{10} s^{-1}, which is exactly the same as the originally chosen value. The same procedure is shown for T_1=300 K and T_2=340 K, with ω_p= 70 Hz in Figure (20). The same value for $N_c\nu\sigma$ is

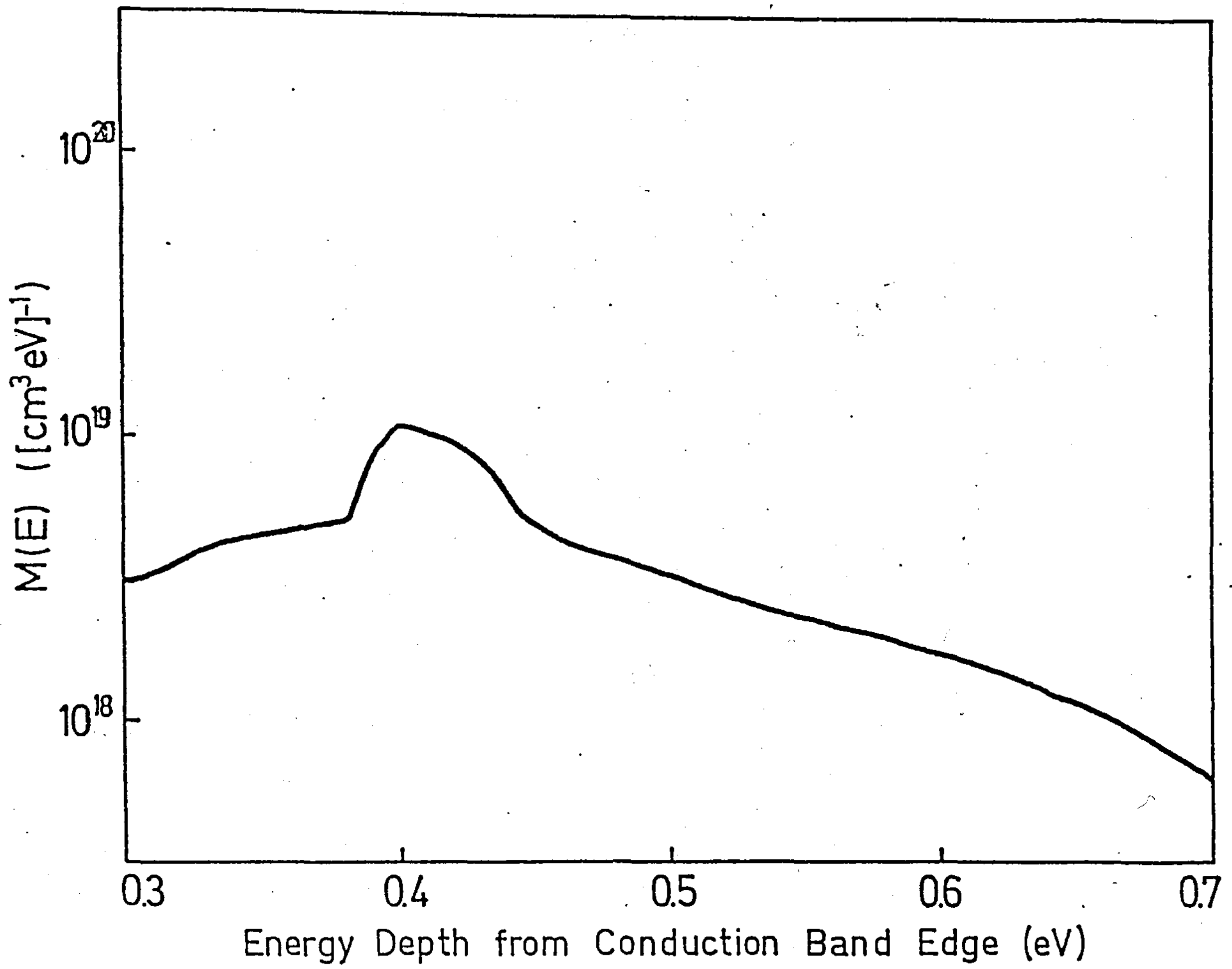

FIGURE (16) The density of state distribution used in the simulation.

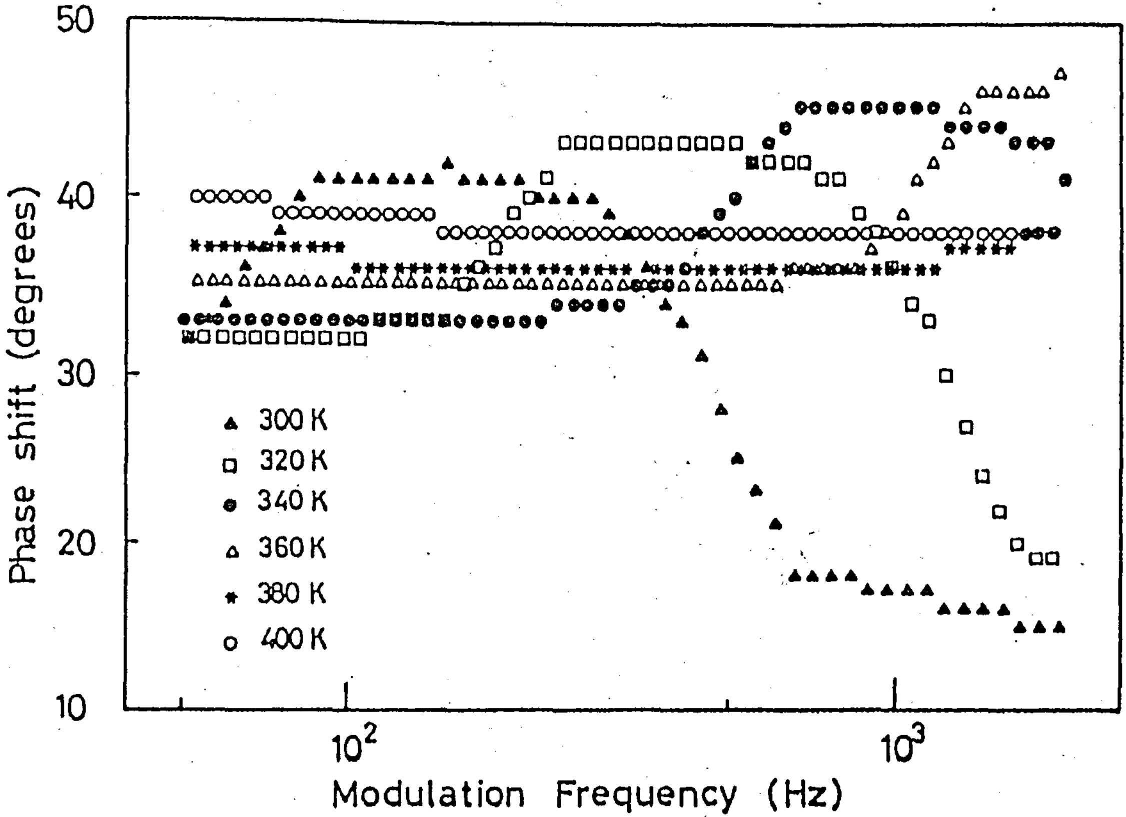

FIGURE (17) Modulation frequency dependence of the phase shift values for several temperatures.

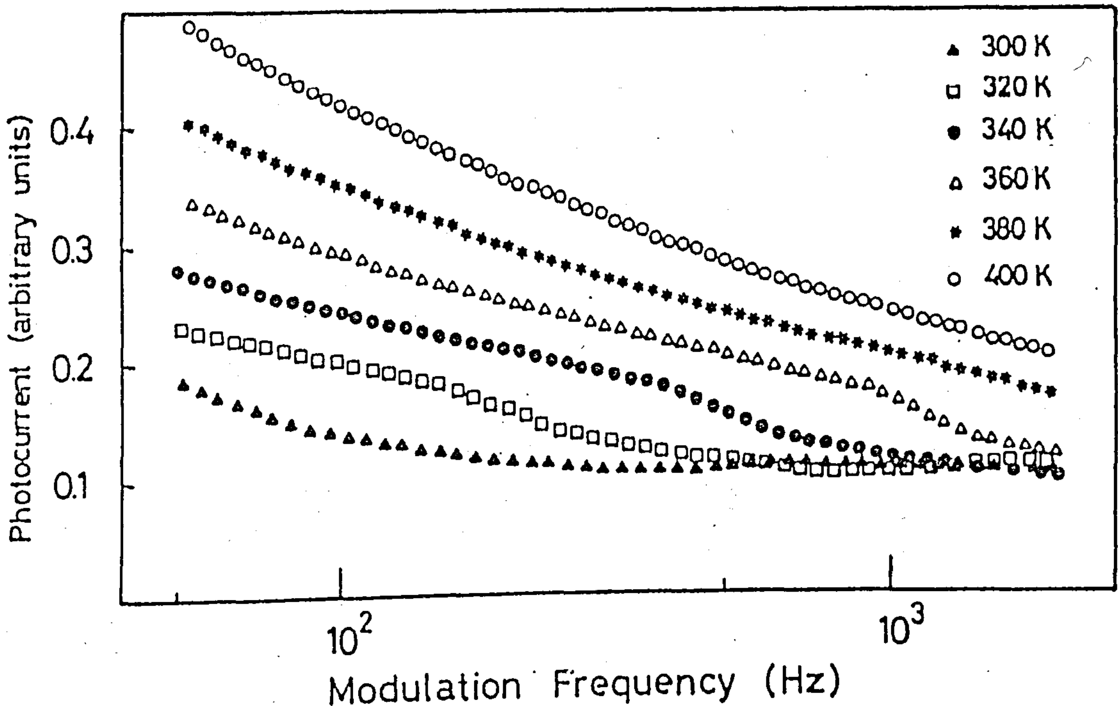

FIGURE (18) Modulation frequency dependence of the intensity of photocurrent values for several temperatures.

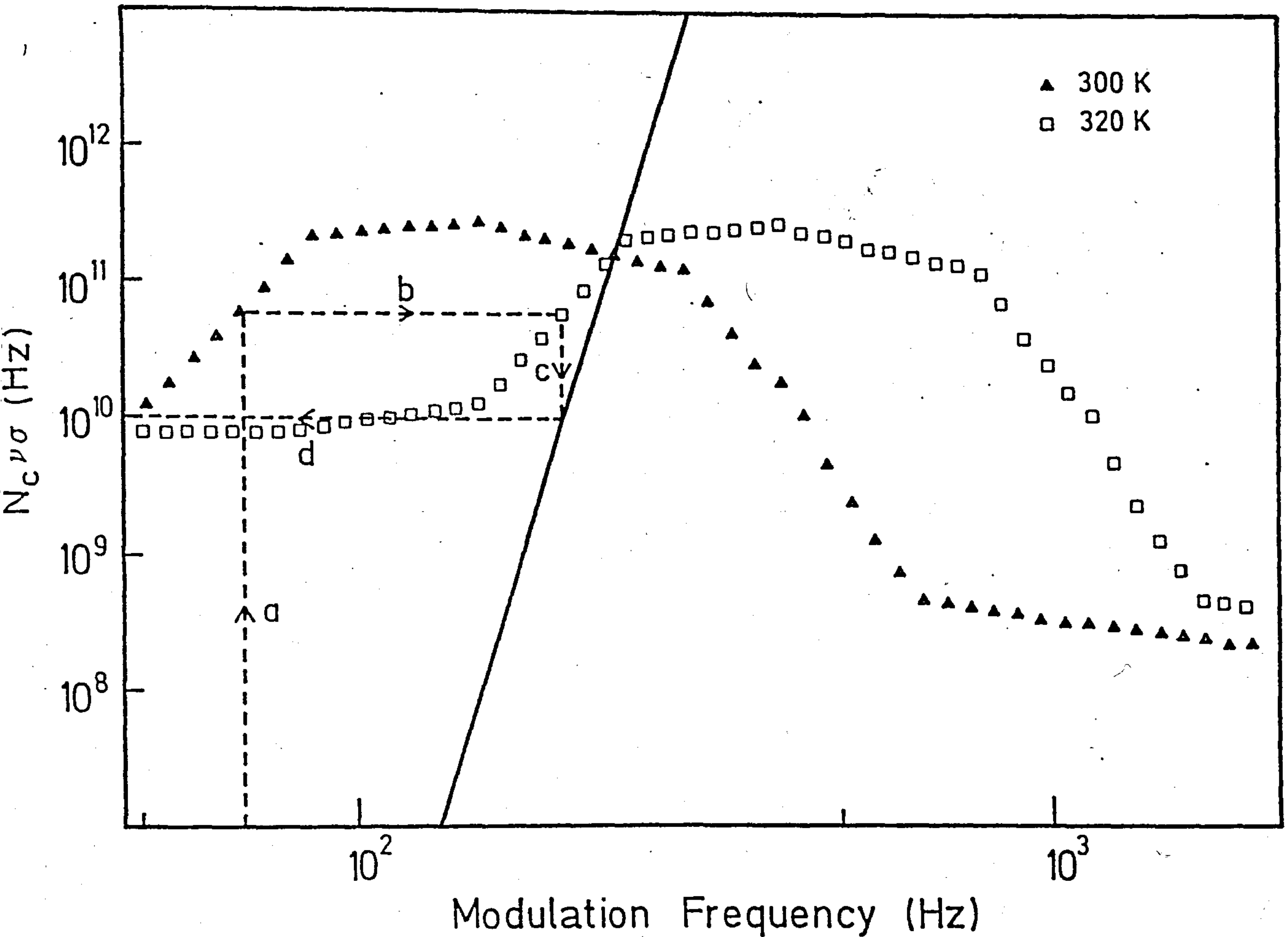

FIGURE (19) Determination of $N_c\sigma\nu$ graphically. The solid line represents Equation (5.21) with ω_p = 70 Hz, T_1 = 300K, and T_2 = 320K. γ spectra at these two temperatures are superimposed on this line. Dashed lines represent (a) γ_{1p} corresponding to 70 Hz, (b) the equivalent ω_q, (c) the equivalent γ_{2q}, and (d) the corresponding value of $N_c\sigma\nu$.

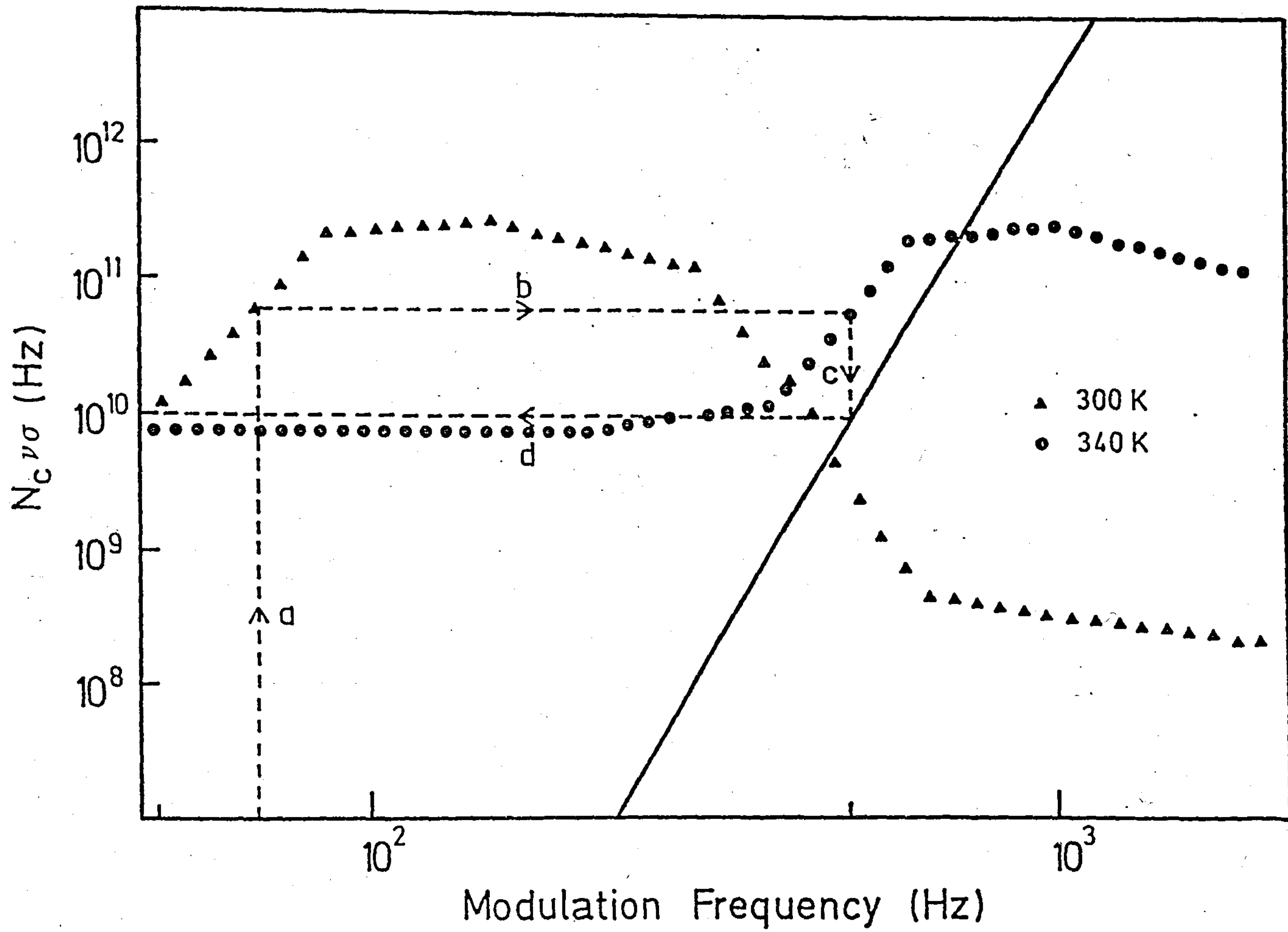

FIGURE (20) Determination of $Nc\sigma\nu$ graphically from γ spectra at temperatures 300K and 340K.

obtained.

Figure (21) shows the frequency spectra of the α values at different temperatures. The dashed lines represent the determination of the normalized coefficient for C_2 which corresponds to T_2=320 K for an arbitrarily chosen C_1 at T_1=300 K. The ω,T pairs that correspond to the same energy have been calculated above as (70 Hz, 300 K) and (202 Hz, 320 K). α_{1p} and α_{2q} representing these pairs are determined from the graph, and in turn are used in Equation (5.25) to determine C_2. This procedure is repeated for the other normalization factors of each temperature spectra. The normalization constants, together with the determined $N_c \nu \sigma$ can now be used in Equation (5.20) to determine the DOS, $M(E_{nj})$, corresponding to E_{nj} energy levels.

Figure (22) shows the final DOS distribution calculated from the data generated in accordance with the procedure described above. With a frequency range of 50-2000 Hz and a temperature range of 300-400 K, an energy region of 250 meV was covered. The result is in perfect agreement with the original curve. The energy axis has been determined exactly by the use of $N_c \nu \sigma$ calculated from the γ spectra. When generating the data for the hypothetical curve given in Figure (16), intentionally different C_n's were taken for each temperature Tn. The $N_c C$ values taken at each temperature are given in the inset of Figure (22).

When analyzing experimental data through the use of the intensity of photocurrent together with the phase shift values it is very important to determine whether or not the experimental conditions have been kept identical at all temperatures. If not, all C_n's must be normalized through the use of α spectra of different temperatures according to arbitrarily chosen C_1. Failure to do so will result in a vertical displacement of the DOS curves of different temperatures. An example of such displacement of curves is given in Figure (23) where instead of the varying $N_c C$'s used to

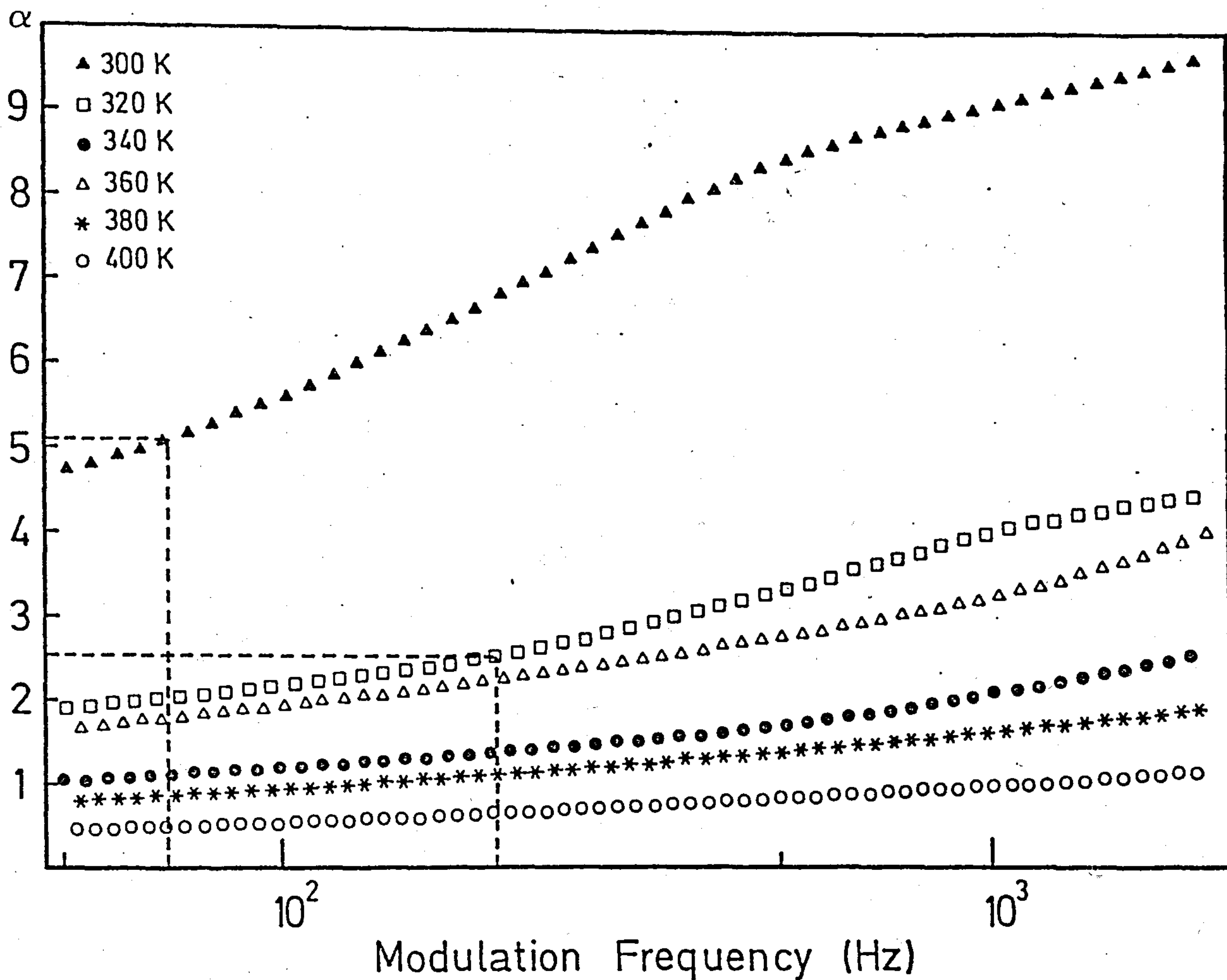

FIGURE (21) Modulation frequency dependence for α's at different temperatures. The dashed lines show the determination of the normalization coefficient (α_1/α_2) for C_2 which corresponds to T_2 = 320K for arbitrarily chosen C_1 value at T_1 = 300K.

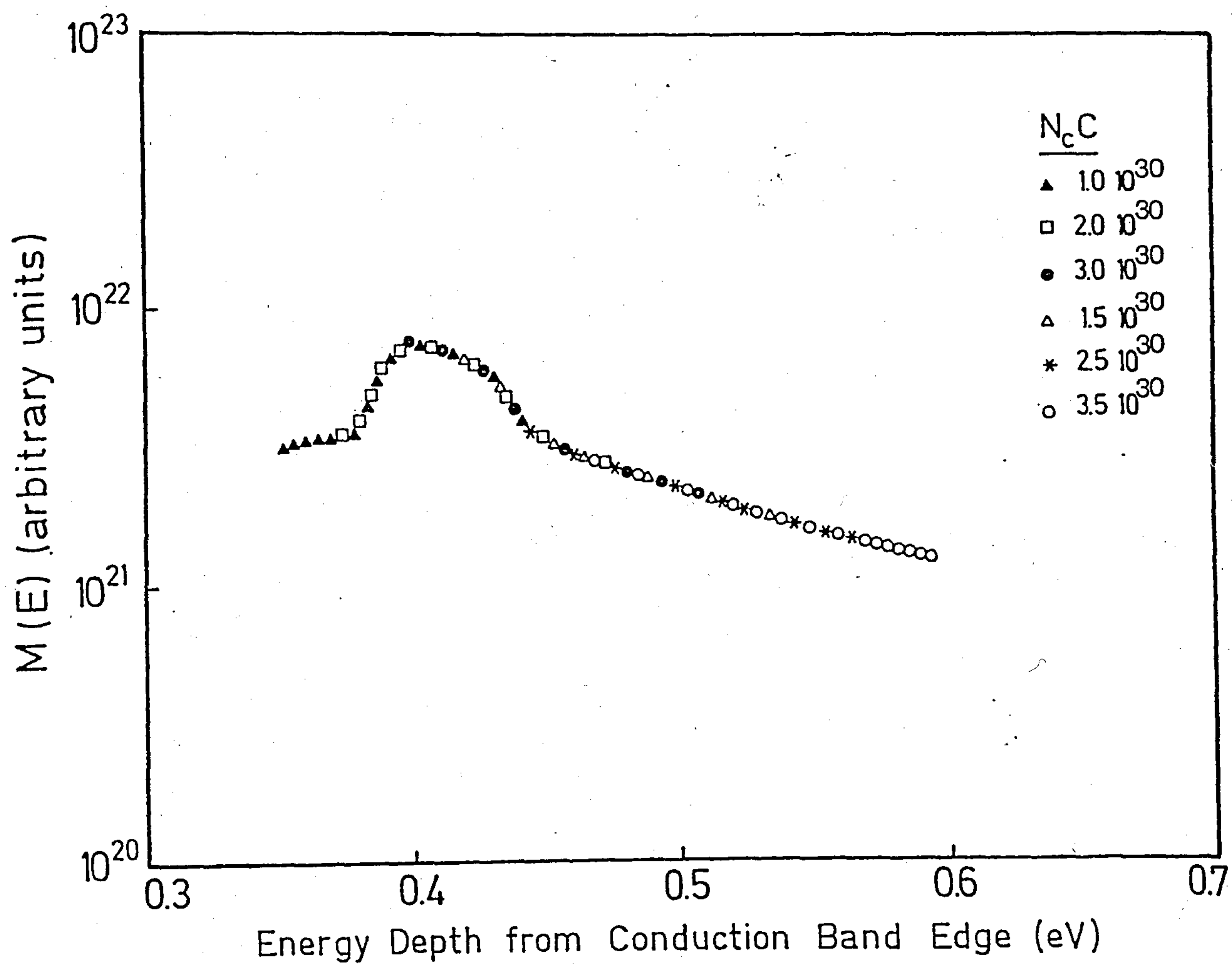

FIGURE (22) Final energetic distribution of density of states obtained by using the procedure described in the text. The NcC values used at each temperature are indicated.

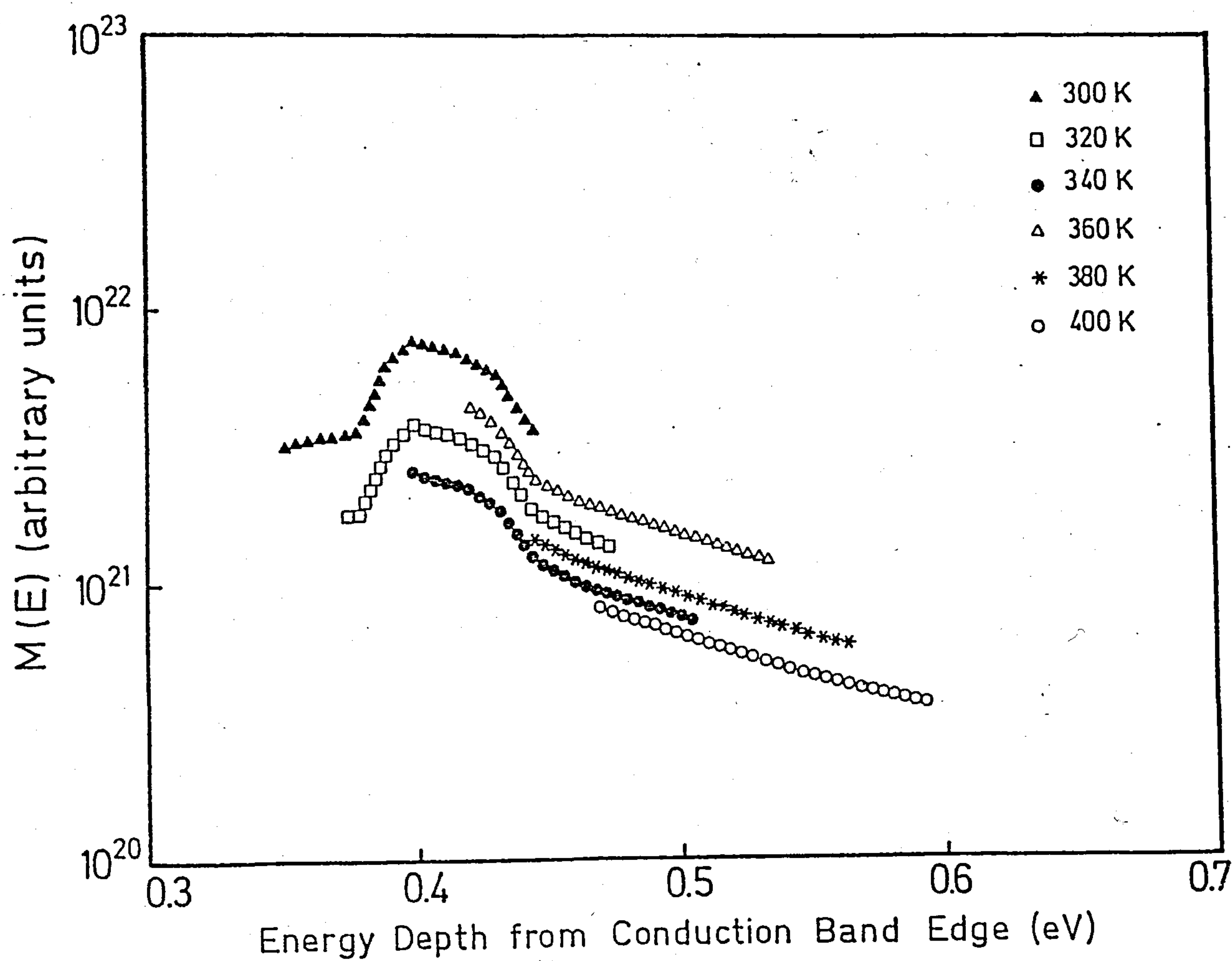

FIGURE (23) Energetic distribution of density of states for the case where N_cC is taken to be (1×10^{30}) for all M(Enj) calculations.

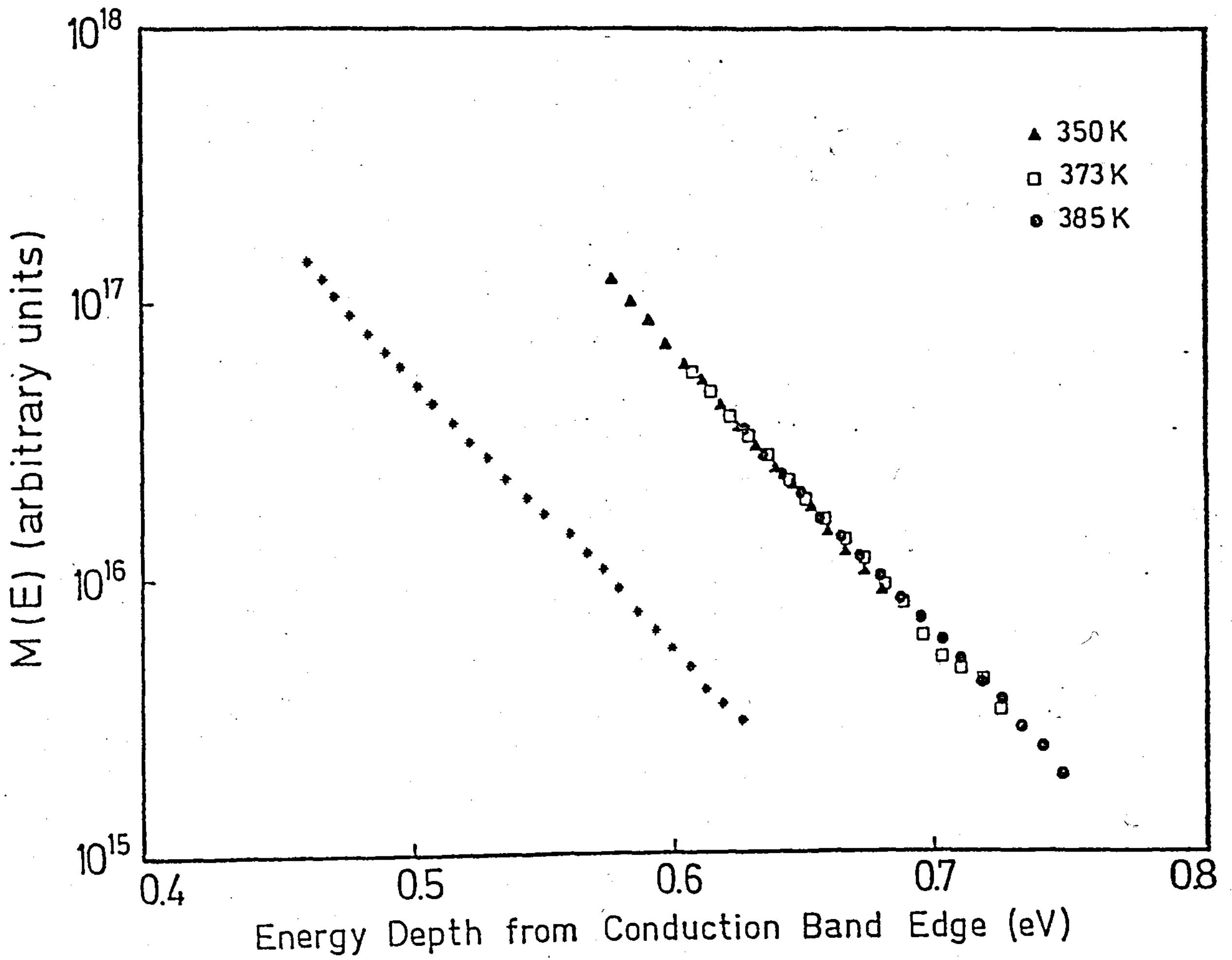

FIGURE (24) The distribution of density of states for an a-Si:N alloy film. The curve on the left is the original curve of White et al.(45), and the curve on the right represents the DOS distribution obtained by the method described in the text.

produce Figure (22), $N_c C$ is taken to be constant for all $M(E_{nj})$ calculations.

Recently White et al. have applied the PSAMP method to determine the DOS distribution in amorphous silicon-nitrogen alloy films(45). Their DOS curves lack a characteristic peak, and they determine their energy axis by using an arbitrary value for the attempt-to-escape frequency $N_c \nu \sigma$. We have applied the procedure described above to their ϕ and I spectra data at 350, 373, and 385 K and we obtained a value of $4.0 \times 10^{12} \pm 1.3 \times 10^{12}$ s^{-1} for $N_c \nu \sigma$.

As can be seen from Figure (24), the DOS curve that resulted using our method has exactly the same shape as theirs. Their arbitrary choice of a value of 10^{11} s^{-1} for $N_c \nu \sigma$ results in a DOS distribution roughly between 0.45-0.63 eV below the conduction band. However, calculations based on the above method shift their DOS distribution towards the Fermi level, placing it approximately between 0.56-0.75 eV below the conduction band.

C. Sensitivity Analysis of the PSAMP Method(12)

In order to determine the sensitivity of the PSAMP method to fine structural features in the DOS, four DOS distributions were considered as is shown in Figure (25). We found it appropriate to study these DOS distributions for two reasons: firstly because they differ from each other in the degree of fine scale structure and secondly because these curves have been used previously in the sensitivity analysis of the field effect method and therefore a basis for meaningful comparison exists.

In the simulation, only the region between the conduction band and the Fermi level was considered. The energy scale was divided into increments of 2 meV and the corresponding M(E) values were read from the graph. For each

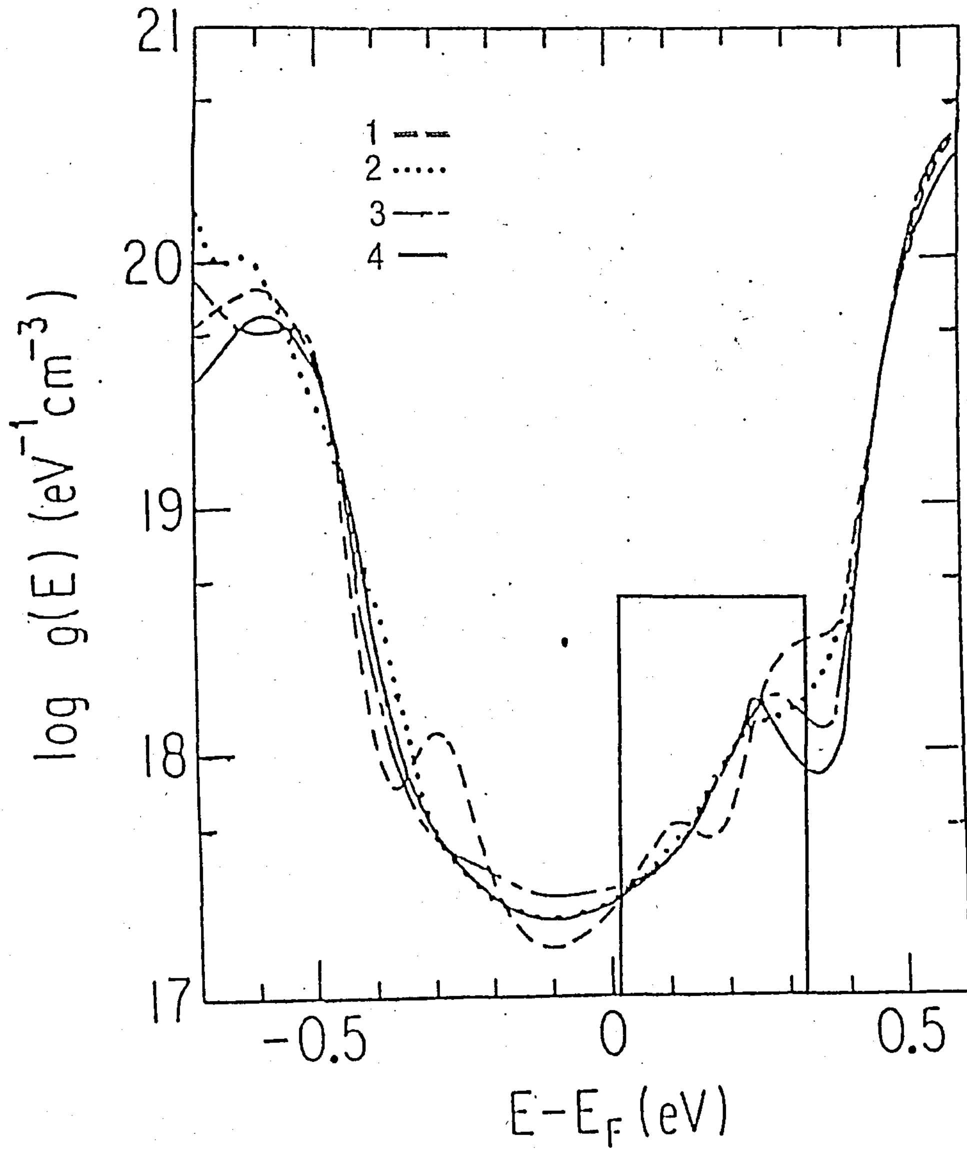

FIGURE (25) Four density of states distributions used in the simulation(49).

distribution five temperature values of 250 K, 290 K, 330 K, 370 K, and 400 K and a frequency range of 50 to 2000 Hz were used. These values enable us to cover an energy region of 303 meV from the Fermi level. Since the fine structure in the distributions occurs within this region, it was considered to be sufficient for analysing the sensitivity of the method. However, it would be possible to cover the whole region by extending the temperature and frequency ranges considered.

The raw data to be measured during the experiment are the phase shift and photocurrent values determined with respect to modulation frequency at different temperatures. These ϕ_j and I_j values, corresponding to the frequencies of 50-2000 Hz are calculated using Equations (5.6), (5.13), (5.14), (5.15), (5.16), (5.18) and (5.20) for each temperature. The parameters used in the calculations are $N_c \nu\sigma = 10^{-10}$ s^{-1} and $(\tau_{RO}\sigma\nu)^{-1}=6x10^{16}$ cm^{-3}. These values were determined in the process of finding the best fit to the original curve. $N_c C$ is arbitrarily taken to be 10^{30}. As examples of the calculated phase shift and photocurrent spectra, only those obtained for 250 K and 330 K are given in Figures (26), (27), (28), and (29) respectively. Since $N_c \nu\sigma$ is taken to be the same for all the DOS distributions, these ϕ and I values correspond to the same energy range. The photocurrent values given in Figures (28) and (29) are normalized with respect to the smallest photocurrent value which is arbitrarily taken to be 0.1.

Phase shift and photocurrent values of Figures (26) and (28) correspond to the energy range between 0.109 eV and 0.214 eV and those in Figures (27) and (29) to 0.228 and 0.307 eV of Figure (25). According to Equation (5.6), the higher the frequency the lower the energy from the conduction band, that is the higher the energy from the Fermi level. Around 0.300 eV from the Fermi level where the DOS distributions 1 and 4 are very distinctly separated from each other and 2 and 3 overlap, the phase shift spectra at 2000 Hz corresponding to the same energy level, in Figure (26), show

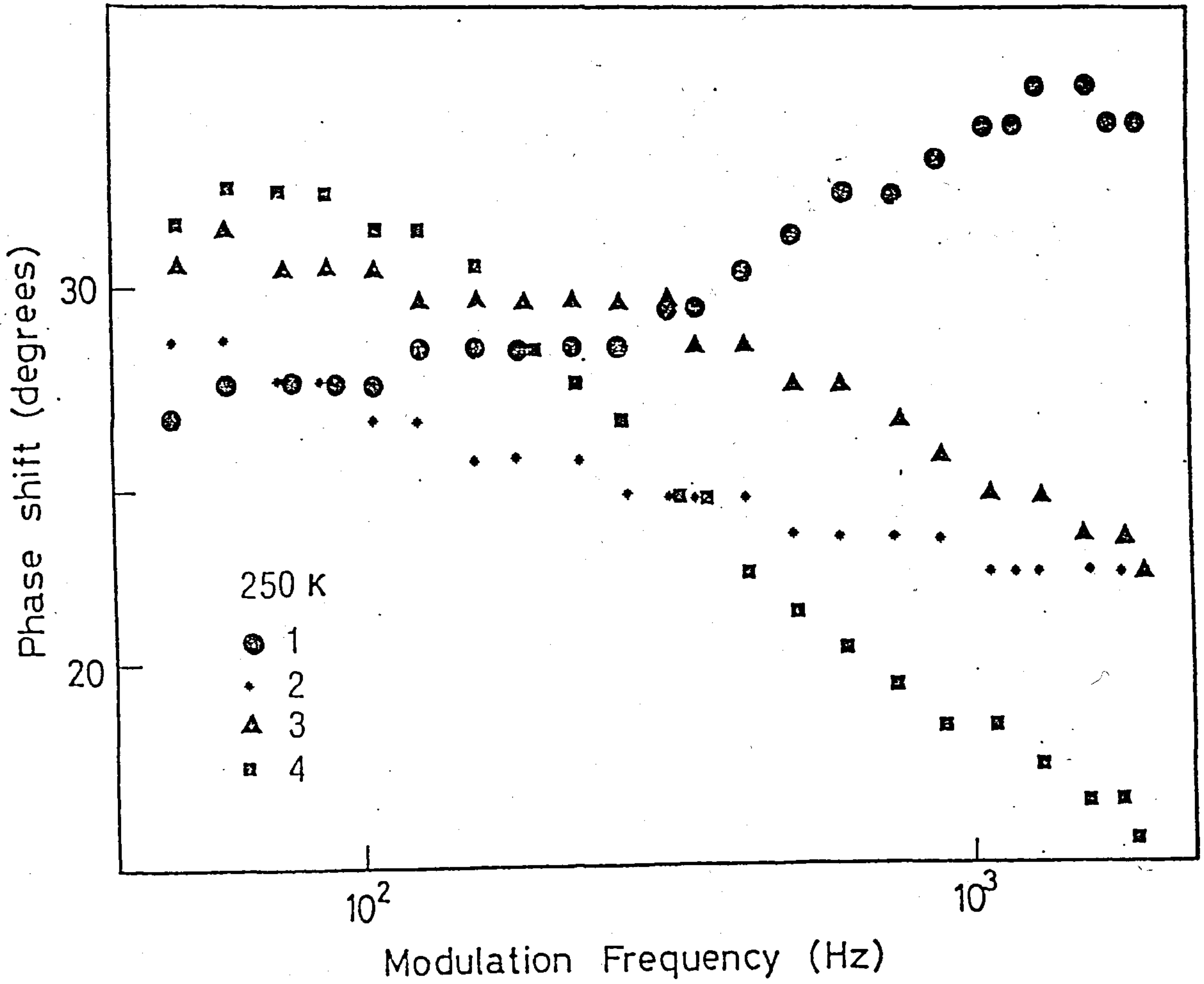

FIGURE (26) Modulation frequency dependence of the calculated phase shift values for 250K.

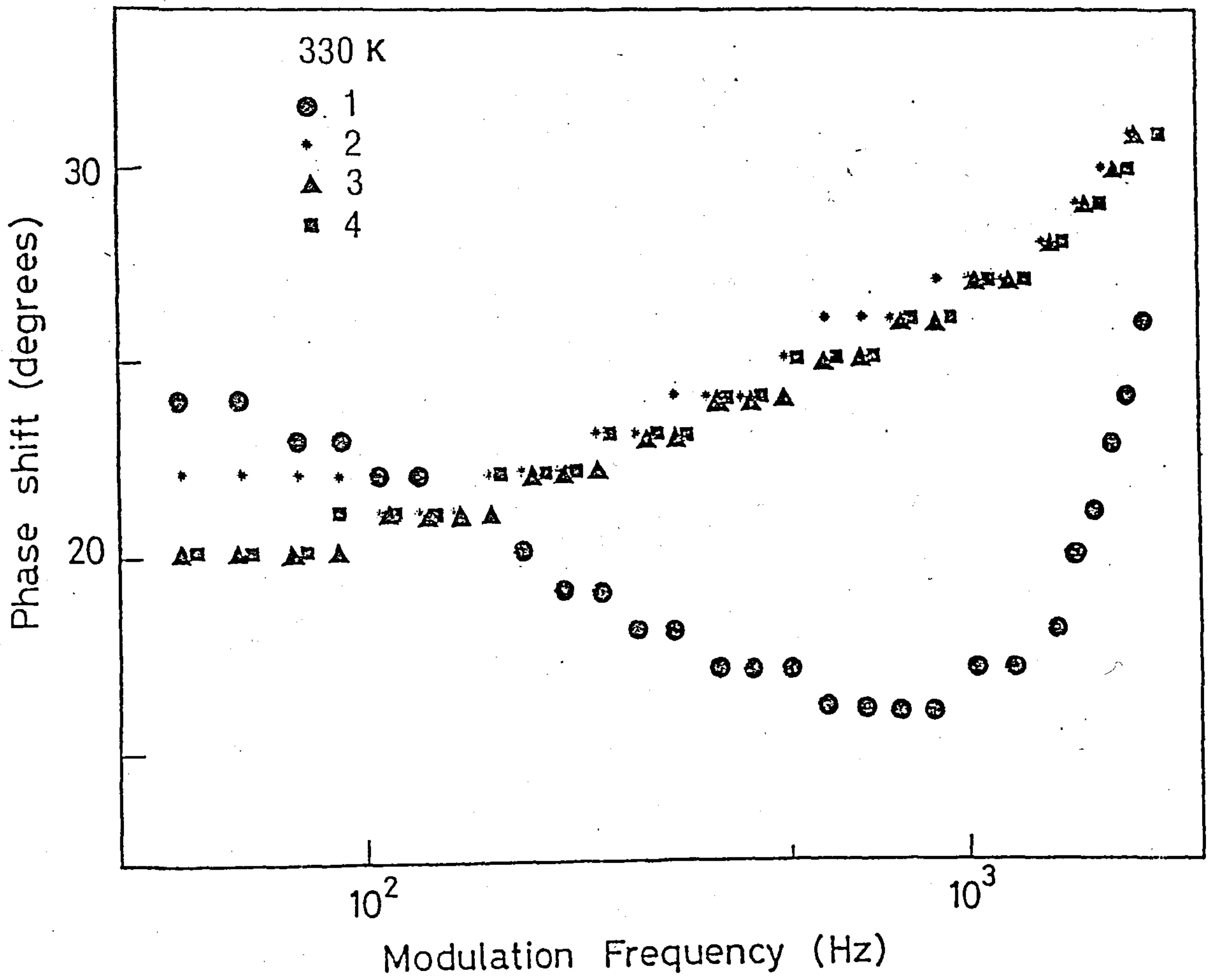

FIGURE (27) Modulation frequency dependence of the calculated phase shift values for 330K.

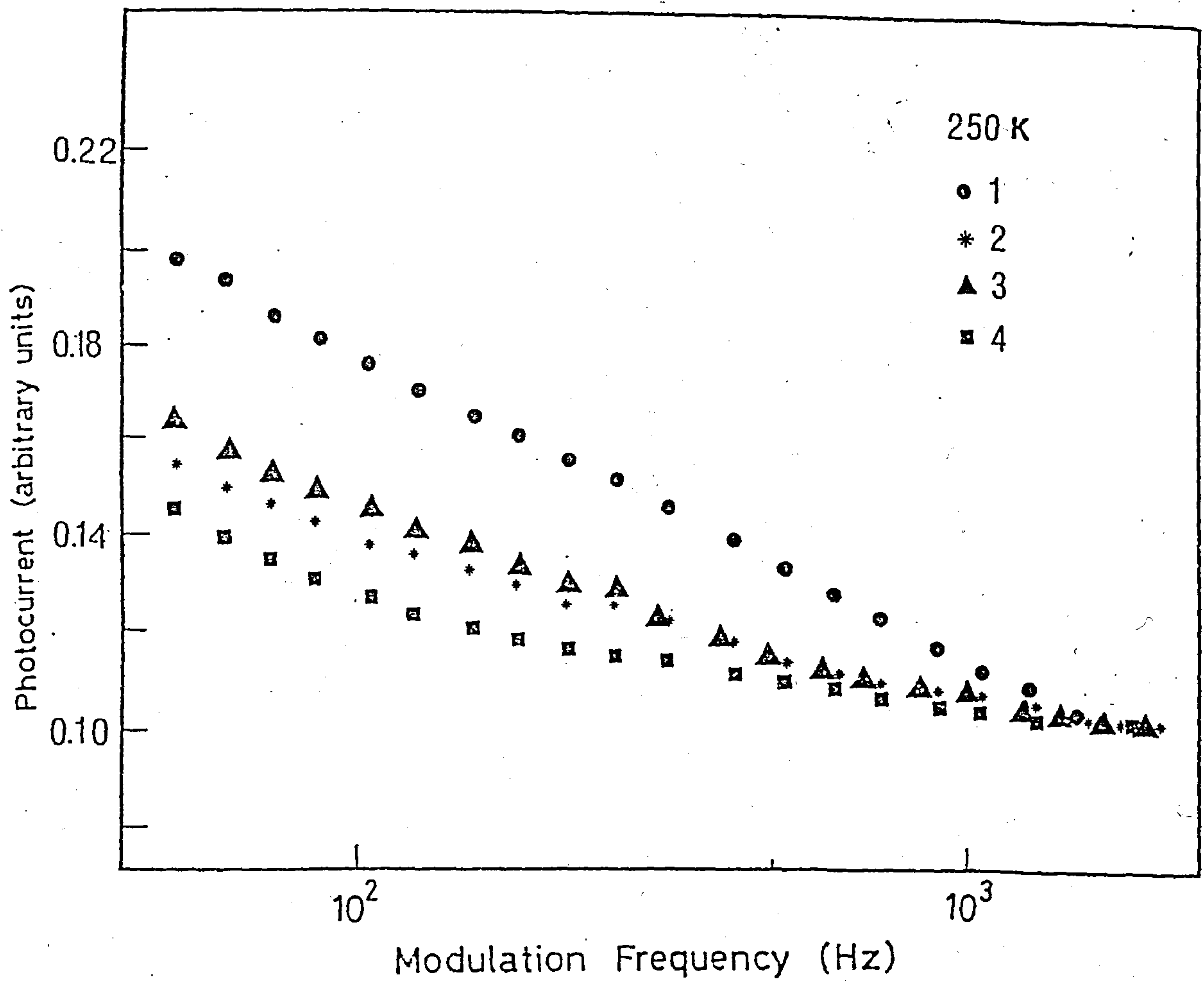

FIGURE (28) Modulation frequency dependence of the calculated photocurrent values for 250K.

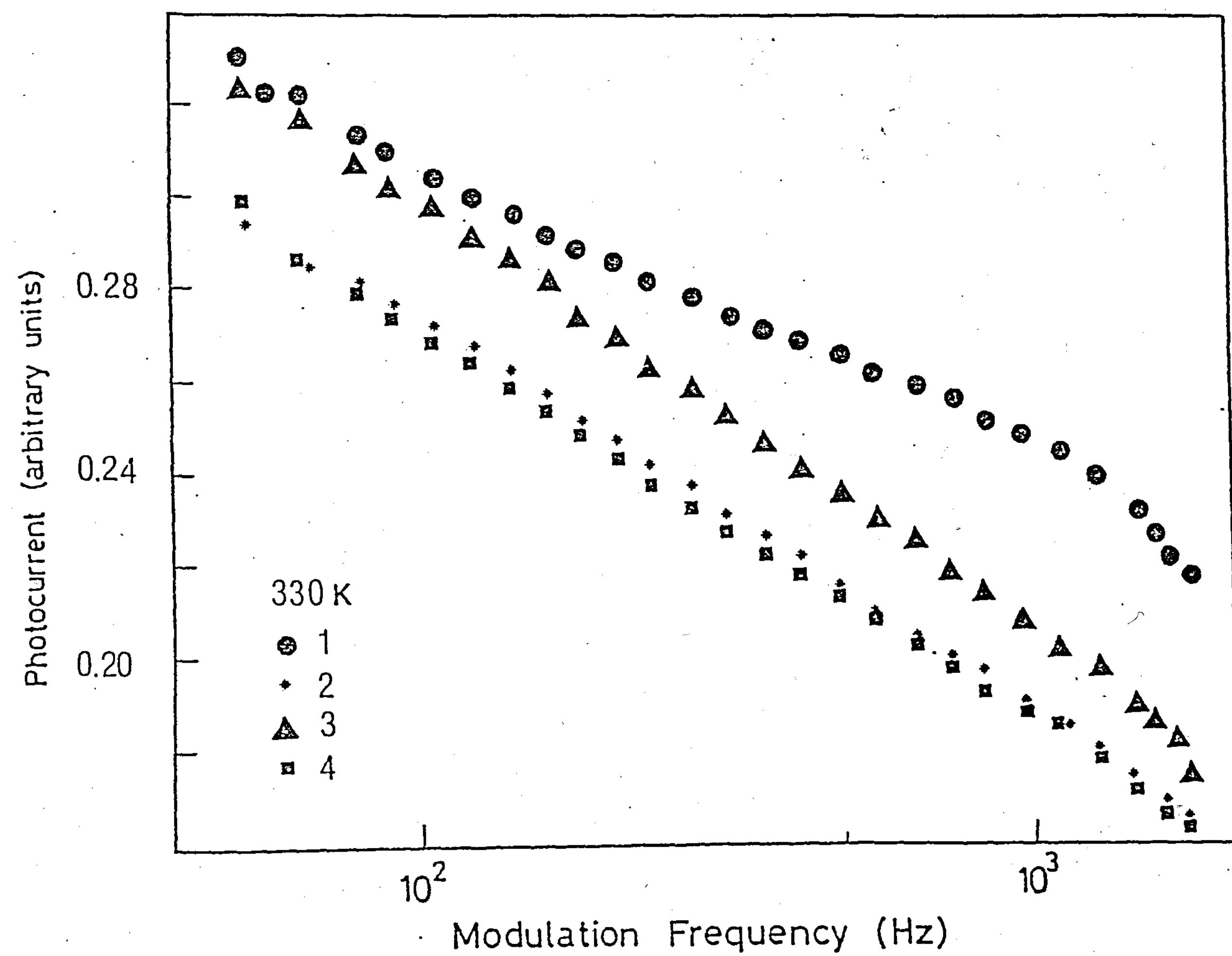

FIGURE (29) Modulation frequency dependence of the calculated photocurrent values for 330K.

exactly the same behavior. At about 0.260 eV, curves 1,3, and 4 cross each other and 2 is slightly below them; so are the phase shift spectra around 200 Hz corresponding to this energy. Around 0.170 eV curves 2,3, and 4 coincide with each other and only curve 1 is distinctly below the other three; and around 0.130 eV all four curves coincide. As can be seen from Figure (27), the phase shift spectra follow the same pattern; 0.174 eV and 0.130 eV corresponding to 500 and 106 Hz respectively. Since the photocurrent spectra of Figures (28) and (29) change slowly and monotonically, the variations in the phase shift values, according to (5.18) and (5.20), clearly indicate the distinct shapes of the DOS distributions. Hence, even within the limits of experimental error, which is around ±1 degree for the phase shift and around 0.1% for the photocurrent, the distinctiveness of these measurements is still valid. The final DOS distributions, given in Figure (30), which is reconstructed from the calculated "data" are in perfect agreement with the original curves. The shift in the M(E) values of a factor of about 10^3 with respect to the original curve is due to the arbitrary value chosen for $N_C C$ which apears in Equation (5.20).

The same distributions of Figure (25) were considered in a simulation for the field-effect data(49) and the results are given in Figure (31). Figures (32) and (33) show the distributions considered and the results obtained in a simulation study for the C-V method(49). In both cases the results show very little difference in the expected spectra of these distinctly distinguishable curves. This indicates that both the field-effect and C-V methods are very limited in distinguishing such features in the DOS distributions.

Another method that has been shown(7),(50) to be sensitive to fine structures in the DOS distributions is the DLTS measurement technique. However, this method has been successfully applied only to doped samples and its instrumentation and analysis are rather complex compared with the other methods. By contrast, PSAMP can not only be successfully

applied to all kinds of pure, hydrogenated and doped amorphous structures, it also does not require any assumption about a distribution of states before analysing the experimental data, and as shown above it is very sensitive to fine structural features of the DOS distributions.

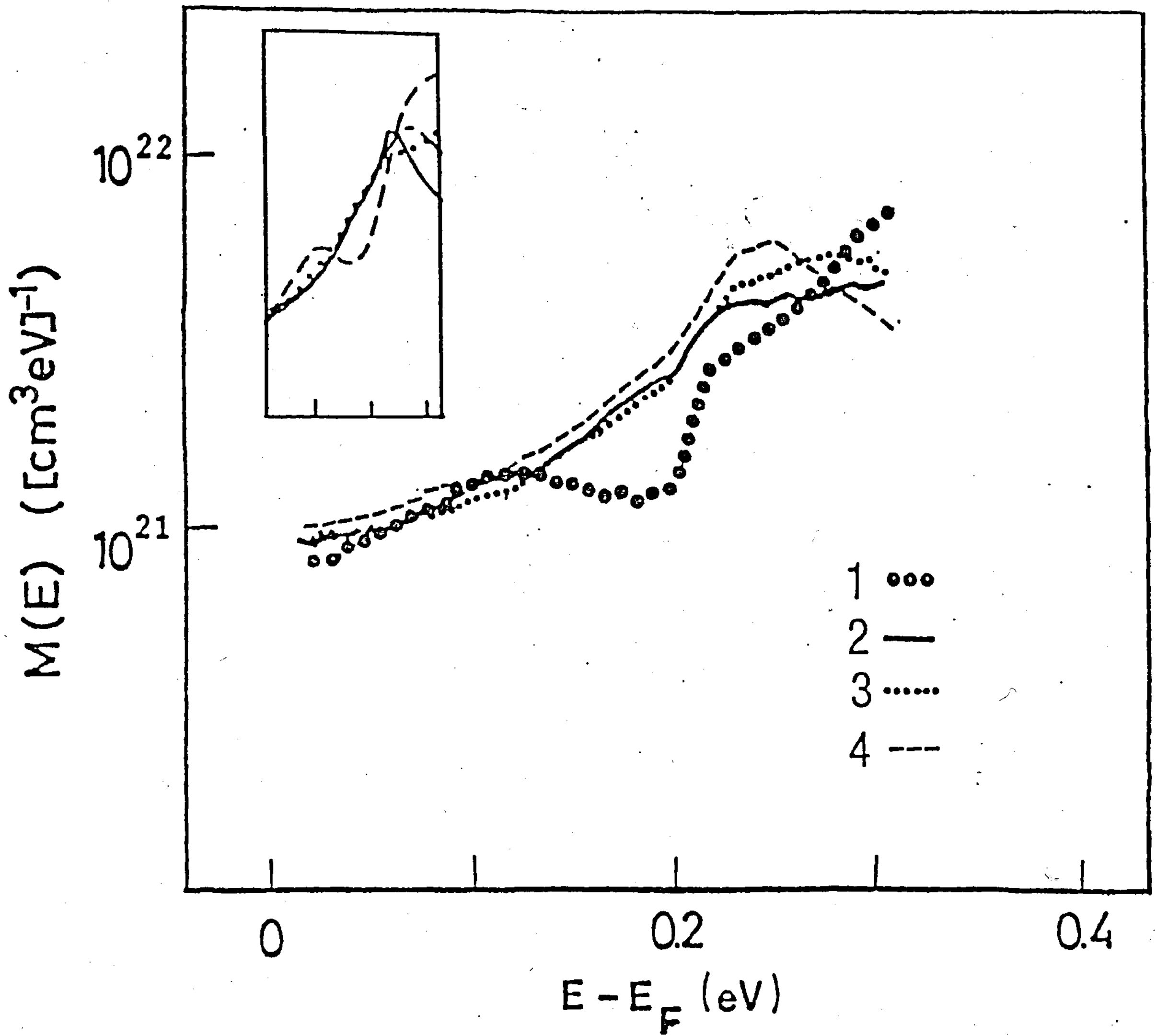

FIGURE (30) Final energetic distributions of M(E) for four DOS distributions. The same energy for the original DOS distributions are shown in the inset.

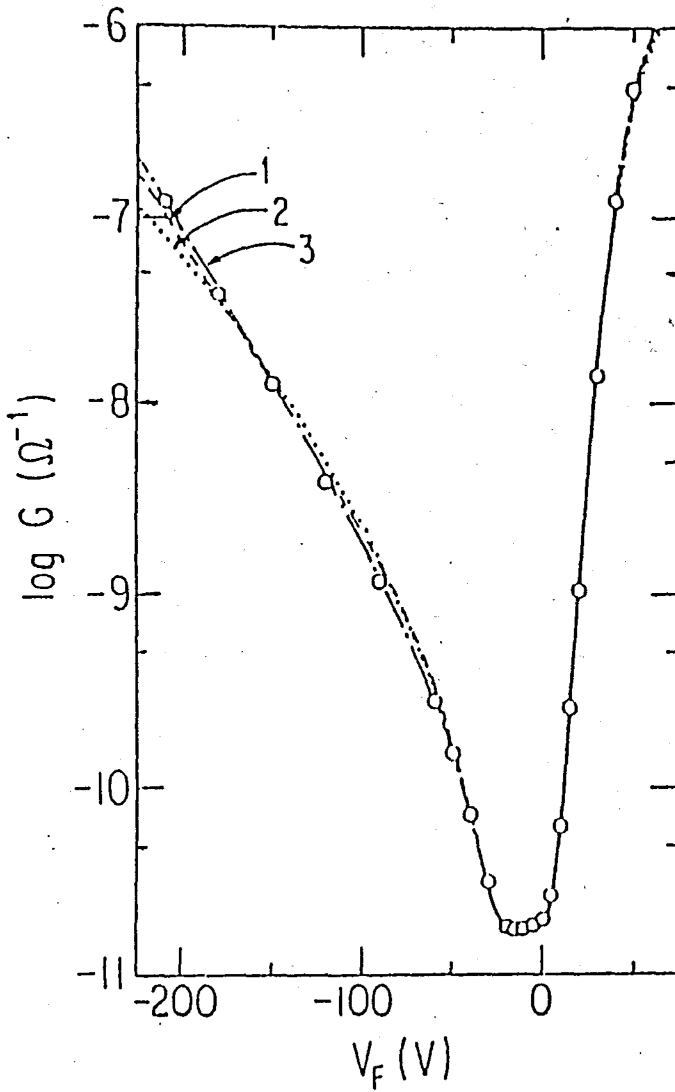

FIGURE (31) Field effect "data" generated from the DOS curves of Figure (25),(49).

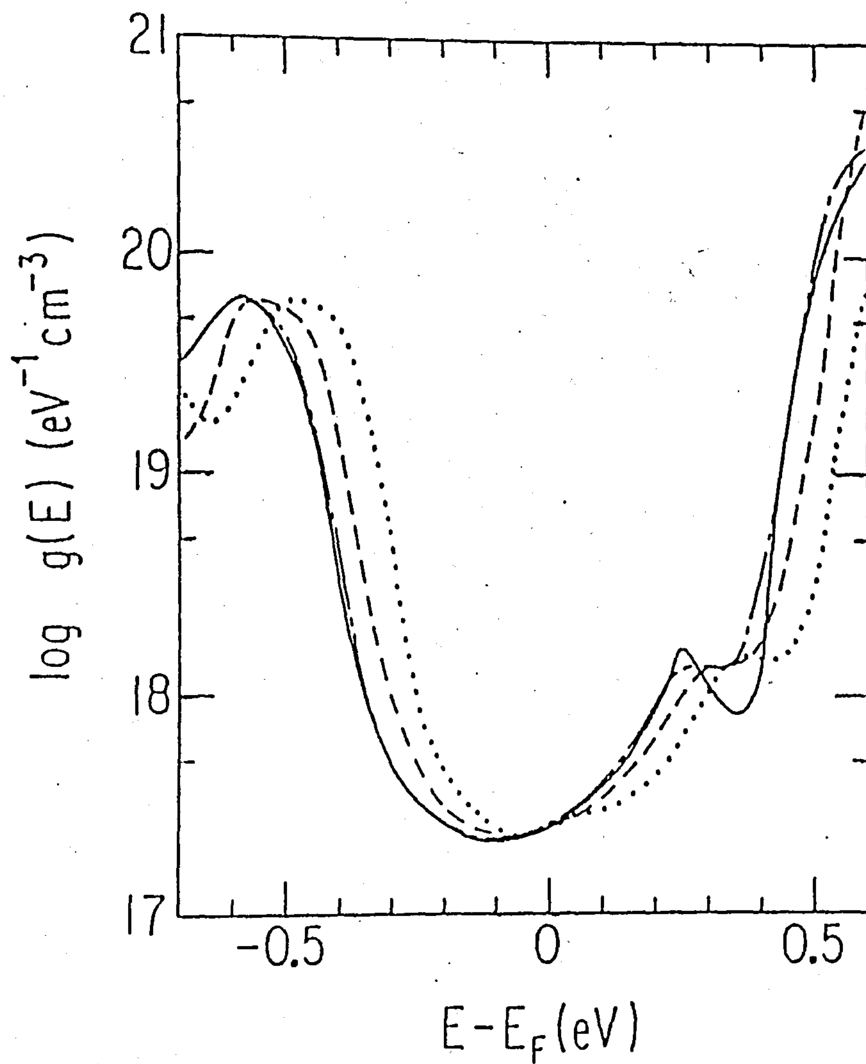

FIGURE (32) DOS distributions used in the simulation for the C-V method(49).

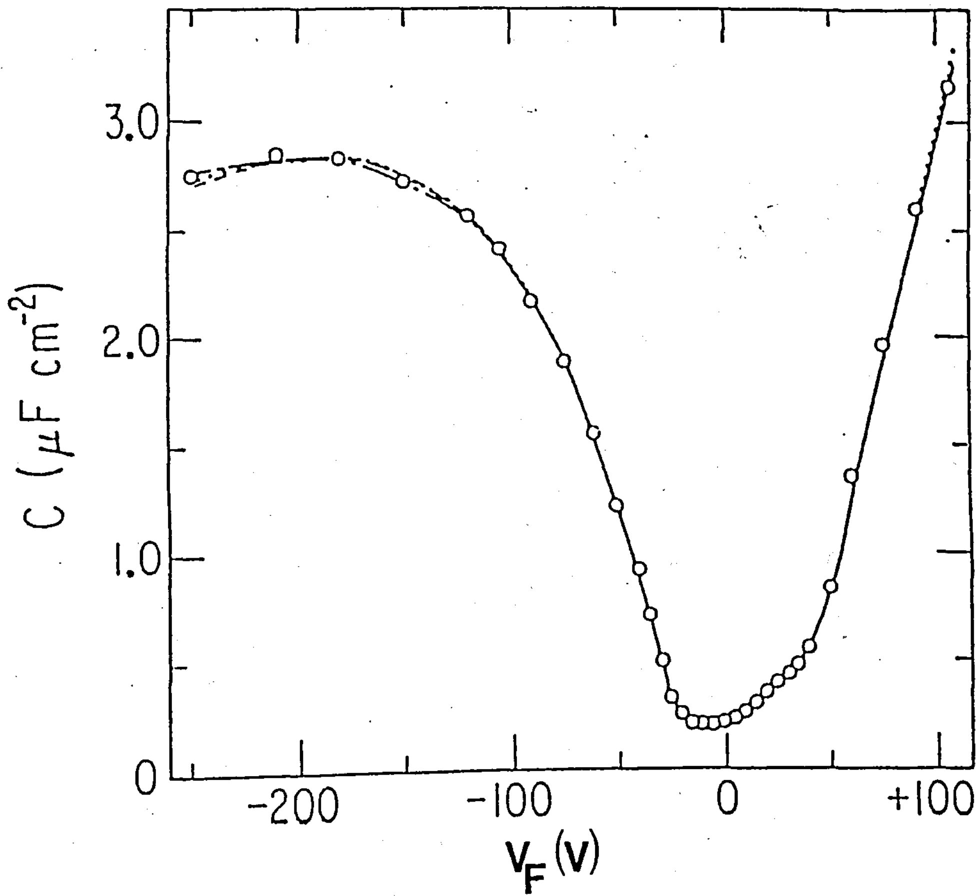

FIGURE (33) C-V "data" generated from the DOS curves of Figure (32),(49).

VI. CONCLUSION

In the first part of the thesis we have given the results of the d.c. and a.c. measurements performed on evaporated a-Si films.

In order to analyze the frequency and the temperature dependence of the a.c. conductance in terms of the classical models like the QMT, the CBH, and the large polaron tunneling model; we have subtracted the d.c. component from the measured conductance. Since between 77 K and 250 K the samples obey the $T^{-1/4}$ law and between 250 K and 400 K the activation energy (around 0.3 eV) is less than half of the expected mobility gap of around 0.6 eV we cannot claim that the d.c. conduction involves band processes. Hence both a.c. and d.c. conductions may involve interactions between localized states, and Equation (2.35) is not justified. Nevertheless, we have shown that a separation of the conductivity into a.c. and d.c. parts is still technically possible.

We have found no result supporting the QMT model. The temperature dependence of s and $\sigma(\omega,T)$ agree to a certain extent with the predictions of the CBH model below 200 K. However the experimental results show that both s and $\sigma(\omega,T)$ are more strongly temperature dependent above 200 K than the CBH model predicts. Even though Reider's modification of including variation of site energies increases the temperature dependence of $\sigma(\omega,T)$, the increase is not as strong as our data show. Long and Shimakawa attribute similar behavior of

their a-Si:H samples to an activated conduction mechanism of tunneling between tail states close to the band edges(51), (52).

Between 150 K and 400 K the behavior of s is better predicted by the large polaron tunneling model but the $N(E_F)$ values calculated from this model are unreasonably high.

We have finally compared our d.c. and a.c. data with the unified theory EPA. The fact that the a.c. results are in perfect agreement with the quasi-universal law predicted by this model is indicative of the same mechanism being responsible for the a.c. and d.c. conductions. However, the quantitative parameters derived from a comparison of the data with the model are not as satisfactory. Both the decay parameter, α, and the rate parameter, R_o, are several orders of magnitude off the "expected" results. The $N(E_F)$ values derived from the EPA d.c. results are slightly low compared with the values given by other researchers for evaporated a-Si. Since the evaporation rate is very low and the resistivities of the films are rather high, this may be due to oxygen incorporation into the films during growth.

In the second part of the thesis we have introduced a new method to determine the exact energy scale of the DOS distribution obtained by the PSAMP method. We have shown that it is possible to avoid introduction of an arbitrary factor in determining the energy scale even for the case where the DOS distribution doesn't have a characteristic peak. The energy scale can also be determined exactly when the experimental conditions are not kept identical at each temperature in the measurements of modulated photocurrent.

Although we have removed the arbitrariness of the energy scale, the arbitrariness in the magnitude of the DOS

remains. An absolute determination of the DOS distribution requires an independent measurement of ν, σ, and τ_{RO}.

One of the important aspects of a method to be used in determining the DOS distribution is its sensitivity to fine structure in this distribution. To determine the sensitivity of the PSAMP method to fine structure in the DOS distribution we have made a simulation and obtained the expected data. The PSAMP method was shown to be very sensitive to structure. A comparison was made with the other commonly used methods and it was shown that the PSAMP method is more sensitive to the fine scale features in the DOS distributions than the other methods available. Hence we can conclude that the PSAMP method is a very effective tool in obtaining the DOS distribution profiles, and unlike the other methods with a limited application range, it has quite a large application range from crystalline to amorphous materials.

BIBLIOGRAPHY

(1) Hamakawa,Y., "Recent Advances in Amorphous Silicon and its Technological Applications," Tetrahedrally-Bonded Amorphous Semiconductors, Ed. D.Adler, and H.Fritzsche, Plenum Press New York, pp.513-530, 1986.

(2) Sah,C.T., L.Torbus, L.L.Rosier, A.F.Tasch, J.R., "Thermal Smission Rates of Carriers at Gold Centers in Silicon," Solid-State Electronics, Vol.13, p.759, 1970.

(3) Lang,D.V., J.D.Cohen, J.P.Harbison, "Measurements of the Density of Gap States in Hydrogenated Amorphous Silicon by Space Charge Spectroscopy,", Physical Review B, vol. 25, no.8, p.5285, 1982.

(4) Spear,W., P.G.LeComber, "Investigation of the Localized State Distribution in Amorphous Silicon Films," Journal of Non-Crystalline Solids, Vol.8-10, pp.727-738, 1972.

(5) Hirose,M., T.Suzuki, G.H.Döhler, "Electronic Density of States in Discharge-Produced Amorphous Silicon," Applied Physics Letters, Vol.34, No.3, pp.234-236.

(6) Oheda,H., "Phase Shift Analysis of Modulated Photocurrent: Its Application to the Determination of the Energetic Distribution of Gap States," Journal of Applied Physics, Vol.52, No.11, pp.6693-6700, 1981.

(7) Cohen,J.D., "Density of States from Junction Measurements in Hydrogenated Amorphous Silicon," Semiconductors and Semimetals, Vol.21, Part C, Ed. J.I.Pankove, Academic, London, p.9, 1984.

(8) Aktaş,G., Y.Skarlatos, "Determination of the Gap Density of States in Amorphous Silicon by Phase Shift Analysis of the Modulated Photocurrent," Journal of Applied Physics, Vol.55, No.10, p.3577, 1984.

(9) Oheda,H., S.Yamasaki, T.Yoshida, A.Matsuda, H.Okushi, and K.Tanaka, "Gap States Distribution of Undoped a-Si:H Determined With Phase Shift Analysis of the Modulated Photocurrent," Japanese Journal of Applied Physics, Vol. 21, No.7, pp.L440-L442, 1982.

(10) Oheda,H., H.Okushi,Y. Tokumaru, and K.Tanaka, "Phase Shift Spectroscopy of Modulated Photocurrent: Its Application to Gold Levels in Crystalline Si," Japanese Journal of Applied Physics, Vol.20, No.9, pp.L689-L692, 1981.

(11) Aktulga,E., C.Zaim Çil, and G.Aktaş, "Phase Shift Analysis of Modulated Photocurrent: A New Approach to Determining the Energy Scale," Applied Physics A, Vol.48, p.517, 1989.

(12) Aktaş,G., C.Z.Çil, and E.Aktulga, "Sensitivity Analysis of the Modulated Photocurrent Method," Applied Physics A, Vol.48, p.237, 1989.

(13) Adler,D., Defects in Covalent Amorphous Semiconductors, Proceedings of the Kyoto Summer Institute, Ed. F.Yonezawa Springer-Verlag, Berlin, 1981.

(14) Semiconductors and Semimetals, Vol.21, Part C, Ed. J.I. Pankove, Academic, London, 1984.

(15) Spear,W.E., and P.G.Le Comber, "Investigation of the Localized State Distribution in Amorphous Silicon Films," Journal of Non-Crystalline Solids, Vol.8-10, p.727-738, 1972.

(16) Cohen,M.H., H.Fritzsche, and S.K.Ovshinsky, "Simple Band Model for Amorphous Semiconducting Alloys," Physical Review Letters, Vol.22, No.2, pp.1065-1068, 1969.

(17) Abkowitz,M., P.G.Le Comber, and W.E.Spear, "A.c. Conductivity in Amorphous Silicon and Germanium and the Density of States at the Fermi Level," Communications on Physics, Vol.1, pp.175-182, 1976.

(18) Mott,N.F., and E.A.Davis, Electronic Processes in Non-Crystalline Materials, Clarendon Press, Oxford, p.212, 1979.

(19) Fritzsche,H., A Review of Some Electronic Properties of Amorphous Substances, Electronic and Structural Properties of Amorphous Semiconductors, Ed. P.G.Le Comber, and J. Mort, Academic Press, London, pp.55-126, 1973.

(20) Long,A.R., "Frequency-Dependent Loss in Amorphous Semiconductors," Advances in Physics, Vol.31, No.5, pp.553-637, 1982.

(21) Pollak,M., and T.H.Geballe, "Low-Frequency Conductivity Due to Hopping Processes in Silicon," Phys.Rev., Vol.122, p.1742, 1961.

(22) Miller,A., and E.Abrahams, "Impurity Conduction at Low Concentrations," <u>Phys.Rev.</u>, Vol.120, p.745, 1960.

(23) Austin,I.G., and N.F.Mott, "Polarons in Crystalline and Non-Crystalline Materials," <u>Advances in Physics</u>, Vol.21, No.41, 1969.

(24) Pike,G.E., "A.c. Conductivity of Scandium Oxide and A New Hopping Model for Conductivity," <u>Physical Review B</u>, Vol.6, p.1572, 1972.

(25) Elliot,S.R., "A Theory of A.c. Conduction in Chalcogenide Glasses," <u>Philosophical Magazine B</u>, Vol.36, No.12, p.1291, 1977.

(26) Movaghar,B., and W.Shirmacher, "On the Theory of Hopping Conductivity in Disordered Systems," <u>Journal of Physics C</u>, Vol.14, p.859, 1981.

(27) Summerfield,S., and P.N.Butcher, "A Unified Equivalent-Circuit Approach to the Theory of A.c. and D.c. Hopping Conductivity in Disordered Systems," <u>Journal of Physics C</u>, Vol.15, pp.7003-7015, 1982.

(28) Butcher,P.N., R.P.Ferrier, A.R.Long, and S.Summerfield, "Hopping Transport in Tetrahedrally Bonded Amorphous Films via States Near The Fermi Level," <u>Tetrahedrally Bonded Amorphous Semiconductors</u>, Ed. D.Adler, and H. Fritzsche, Plenum Press, New York, pp.325-343, 198 .

(29) Pike,G.E., and C.H.Seager, "Percolation and Conductivity," <u>Physical Review B</u>, Vol.10, p.14, 1974.

(30) Summerfield,S., "Universal Low-Frequency Behavior in the A.c. Hopping Conductivity of Disordered Systems," <u>Philosophical Magazine</u>, Vol.5, No.1, pp.9-22, 1985.

(31) Summerfield,S., and P.N.Butcher, "Universal Behavior of A.c. Hopping Conductivity in Disordered Systems," Journal of Non-Crystalline Solids, Vol.77-78, pp.135-138, 1985.

(32) Knotek,M.L., M.Pollak, T.M.Donovan, and H.Kurtzman, "Thickness Dependence of Hopping Transport in a-Ge Films," Physical Review Letters, Vol.30, p.853, 1973.

(33) Apsley,N., and H.Hughes, "Temperature and Field Dependence of Hopping Conduction in Disordered Systems II," Philosophical Magazine, Vol.31, p.1327, 1975.

(34) Stutzman,M., and J.Stuke, "Paramagnetic States in Doped Amorphous Silicon and Germanium," Solid State Communications, Vol.47, p.635, 1983.

(35) Ehinger,K., S.Summerfield, W.Bauhofer, and S.Roth, "D.c. and Microwave Conductivity of Iodine-Doped Polyacetylene," Journal of Physics C, Vol.17, p.3753, 1984.

(36) Long,A.R., J.McMillan, N.Balkan, and S.Summerfield, "The Application of the Extended Pair Approximation to Hopping Conduction in R.F.Sputtered Amorphous Silicon," Philosophical Magazine B, Vol.58, No.2, p.153-169, 1988.

(37) Çağlayan,B., "An Environmental Chamber Enabling Electrical and Electro-Optic Measurements," M.S.Thesis, Boğaziçi University, 1982.

(38) Çil,C.Z., and G.Aktaş, "Frequency Dependent Conductivity in Evaporated Amorphous Silicon Films," Journal of Non-Crystalline Solids, Submitted to be published, 1989.

(39) Elliot,S.R., "Defect States in Amorphous Silicon, "Philosophical Magazine B, Vol.38, No.4, pp.325-334, 1978.

(40) Reider,G., "Frequency-Dependent Dielectric Behavior of Amorphous Silicon Thin Films," Physical Review B, Vol.20, No.2, pp.607-615, 1979.

(41) Shimakawa,K., A.Watanabe, "Frequency-Dependent Transport in Glow-Discharge Amorphous Silicon, "Philosophical Magazine B, Vol.54, No.5, pp.391-414, 1986.

(42) Mott,N.F., "Conduction in Non-Crystalline Materials," Philosophical Magazine, Vol.19, p.835, 1969.

(43) Chik,K.P., K.C.Koon, "Evidence for Nearest-Neighbour Hopping in Amorphous Silicon," Philosophical Magazine B, Vol.53, No.5, pp.399-405, 1986.

(44) Knotek,M., "Temperature and Thickness Dependence of Low Temperature Transport in a-Si Thin Films: A Comparison to a-Ge," Solid State Communications, Vol.17, p.1431, 1975.

(45) White,J.F., K.C.Kao, H.C.Card, and H.Watanebe, "Gap State Distribution Profiles in Amorphous Silicon-Nitrogen Alloy Films Fabricated at Various Substrate Temperatures," Journal of Non-Crystalline Solids, Vol.85, pp.20-28, 1986.

(46) Fortunato,G., "Determination of Localized State Energy Distribution in a-Si:H By Modulated Photocurrent," Journal of Non-Crystalline Solids, Vol.97-98, pp.739-742, 1987.

(47) Aktaş,G., "Modüle Edilmiş Fotoakım Yöntemi ile Amorf Si - lisyum Filmlerde Yerleşik Durum Yoğunluğunun Belirlenmesi, Ph.D.Dissertation, Istanbul University, 1983.

(48) Aktulga,E., and G.Aktaş, "Phase Shift Analysis of Modulated Photocurrent: Determination of the Energy Scale," Applied Physics A, Vol.45, pp.221-224, 1988.

(49) Goodman,N.B., and H.Fritzsche, "Analysis of Field-Effect and Capacitance-Voltage Measurements in Amorphous Semiconductors," Philosophical Magazine B, Vol.42, No.1, pp. 149-165, 1980.

(50) Cohen,J.D., D.V.Lang, "Is the DLTS Density of States for Amorphous Silicon Correct?," Ibid. Ref.28, pp.299-314.

(51) Shimakawa,K., and A.R.Long, "Frequency-Dependent Loss in Sandwich Samples of Hydrogenated Amorphous Silicon," Philosophical Magazine Letters, Vol.56, No.2, pp.79-84, 1987.

(52) Eşme,I., C.Z.Çil, and G.Aktaş, "Frequency Dependent Conductivity in As_2Se_3 and As_2Se_3+15% Sb," Applied Physics A, accepted to be published, 1989.